

Design localized high concentration electrolytes via donor number and solubility

Juner Chen,^{1,2,6} Han Zhang,^{1,3,6} Changming Ke,^{4,5,6} Shi Liu,^{4,5*} Jianhui Wang^{1,2,3*}

1 Key Laboratory of 3D Micro/Nano Fabrication and Characterization of Zhejiang Province, School of Engineering, Westlake University, Hangzhou, China

2 Institute of Advanced Technology, Westlake Institute for Advanced Study, Hangzhou, China

3 Department of Chemistry, Zhejiang University, Hangzhou, China

4 Key Laboratory for Quantum Materials of Zhejiang Province, School of Science, Westlake University, Hangzhou, China

5 Institute of Natural Sciences, Westlake Institute for Advanced Study, Hangzhou, China

6 These authors contributed equally to this work

*E-mail: wangjianhui@westlake.edu.cn, liushi@westlake.edu.cn

Abstract

The salt-concentrated electrolytes offer superior properties beyond conventional dilute electrolytes yet suffer from high cost and viscosity that hinder their practical applications. A key strategy to address this challenge is to introduce a secondary solvent as a diluent that reduces the salt content while maintaining the local structure of salt-concentrated electrolytes, giving rise to localized high concentration electrolytes (LHCEs). Through a thorough investigation involving ~700 samples, we find that, the dielectric constant of solvent, a widely used parameter for electrolyte design, does not serve as a useful screening criterion for diluents; instead, donor number (DN) is an effective design parameter to achieve LHCE structure, i.e., the primary solvent must have $DN > 10$ and the diluent must have $DN \leq 10$. Correlating DN with solvent solubility leads to a simpler screening rule: Li-salt-insoluble solvents are diluents while Li-salt-soluble solvents become co-solvents. Both DN- and solubility-based design principles can be understood in an atomistic model of LHCE and are applicable to other electrolyte systems.

One-Sentence Summary: Solvents' donor number is a more reliable parameter than dielectric constant to determine the structure and solubility of solution.

Introduction

Lithium-ion batteries, powering various portable electronics and electrically driven transportations, are ubiquitous in our life, yet they are still far from an ideal energy storage device that meets the requirements of ongoing fast developing mobile revolution due to their insufficient energy density and unsatisfying safety property. The capacity and safety limitations in current Li-ion batteries are considerably owing to the electrolyte. State-of-the-art Li-ion electrolytes have a general formula of 1 M (mol L^{-1}) solution of LiPF_6 salt dissolved in a mixed solvent of cyclic ethylene carbonate (EC) and linear carbonate esters. The LiPF_6 salt is Chemically and thermally unstable and the carbonate solvents are highly flammable which strongly dictate the battery performance with a limited working voltage, a narrow operating temperature, and high safety risk. Therefore, alternative electrolytes must be developed to replace these conventional electrolytes in pursuit of high-energy-density and high-safety batteries(1,2).

Recently, salt-concentrated electrolytes have received great attentions because of their superior properties beyond conventional dilute electrolytes(3-6). By simply increasing the salt concentration above a threshold (usually 3-5 M), all the solvent molecules and anions coordinate to Li^+ , resulting in a new solution structure with negligible free-state solvent molecules that is completely different from conventional dilute solution wherein free-state solvent molecules take up the majority(7-11). This remarkable change of solution structure unique to the salt-concentrated electrolytes alters not only the physicochemical properties but also the intrinsic electronic structure, contributing to a new design principle towards various LiPF_6 -free and EC-free electrolytes with advanced properties for next-generation batteries, such as low flammability(11-13), wide electrochemical window(11,14,15), and suppression of dendrite formation and shuttle reactions(16-19). However, concentrated electrolytes suffer from high viscosity and high cost (salts are several times more expensive than solvents), which impede them for practical applications(4-6).

A promising solution to this issue is the introduction of an appropriate diluent to form so-called localized high concentration electrolyte (LHCE), in which the diluent is miscible with the parent concentrated electrolyte but does not coordinate to Li^+ such that the localized solution structure of the parent electrolyte are preserved. Enabled by the unique solution structure, LHCEs inherit advanced properties of concentrated electrolytes while exhibit reduced viscosity and cost, as evidenced by extensive attempts on the sulfur cathode(20-22), lithium metal anode(23-26), and high-voltage lithium-ion batteries(27-30). Despite these remarkable

progresses, almost all the diluents reported are hydrofluoroethers that are even more expensive than the salt. Thereby, it is urgent to develop cheap diluents to reduce the cost of the LHCE.

However, finding an appropriate diluent to realize LHCE relies mostly on the trial-and-error approach. In the research field of electrolytes, dielectric constant (ϵ) is widely regarded as an important parameter for solvents to regulate electrostatic interactions between solution components (e.g., ion-solvent, cation-anion, and solvent-solvent), thus dictating the coordination environment of ions and the dissolution of salts(1,31-33). Take state-of-the-art Li-ion electrolyte as an example, high- ϵ EC is selected for multiple reasons: enhancing Li^+ -EC coordination, increasing the LiPF_6 solubility in the electrolyte, promoting the dissociation of solvated Li^+ , and enabling the formation of protective film on the graphite anode¹. According to this understanding, it is generally believed that a diluent should have a low ϵ such that it cannot compete with primary solvent molecules to coordinate to Li^+ (23,28,34-37). This assumption looks valid at first sight because the most studied diluent of hydrofluoroethers have a lower ϵ compared to many primary solvents (<6 vs. 7~90). Additionally, some studies claimed that a diluent should have a lower polarity and/or donor ability(37-41). However, nearly all previous studies only involve a small number of samples (<10), leaving lots of counterexamples unshown. As we will discuss in this work, many solvents with ϵ , polarity (gauged by dipole moment, μ) and donor ability (gauged by donor number, DN) lower than the primary solvents considerably participate in the coordination to Li^+ , strongly deviating from those assumptions. Therefore, it is of fundamental importance to build up a reliable design principle for LHCEs.

In this work, we applied Raman and Nuclear Magnetic Resonance (NMR) spectrometers to characterize the solution structures of over 500 electrolyte samples that had been diluted by 36 organics with different values of ϵ , μ and DN. We found that the localized solution structure of electrolyte does not show meaningful correlation with ϵ and μ of the solvents but strongly correlates with a critical DN threshold. Specifically, an eligible diluent must have a DN smaller than 10, independent of the type of salt anions and primary solvents. First-principles density functional theory calculations confirmed that the Li-solvent interaction strength scales almost linearly with the DN value of the solvent, while being insensitive to the anion type of the Li-salts. We further proposed that the solvent solubility of Li-salts is a convenient indicator of Li-solvent interaction strength and can be used to search for diluents. This leads to a facile and efficient diluent design principle: Li-salt-insoluble solvents are diluents while Li-salt-soluble solvents become co-solvents. Our finding identifies the key factors determining the localized solution structure, which serves as a principle for fast screening diluents for salt-concentrated

electrolytes, and thus, contributing to the development of low-cost and high-performance LHCEs.

Results and discussion

Preparation and characterization of LHCEs

Lithium bis(fluorosulfonyl)imide (LiFSI) was selected as the salt in this study because it has a decent solubility in both polar and nonpolar solvents and is widely used for salt-concentrated electrolytes in the literatures(5). 36 organic solvents, including ethers, esters, nitriles, alcohols, aromatics and alkanes, were used as primary solvents (termed as Solv.I) or diluent candidates (secondary solvents, termed as Solv.II) for electrolytes preparation; they have a wide range of ϵ (1~90), μ (0~5) and DN (0~30) (See Table 1). Among them, 9 organics were selected as primary solvents (marked in blue in Table 1) because they can dissolve LiFSI in a high content to form concentrated electrolytes. Then, the concentrated electrolytes were mixed with 36 secondary solvents one by one to form diluted solutions with a LiFSI : Solv.I : Solv.II molar ratio of 1 : 2 : 8 (close to 1 M). After that, the Chemical coordination environments of primary solvent and FSI⁻ anion in the diluted solutions were examined by Raman and/or NMR measurements. If the solution structural features of a diluted solution highly resemble those of the parent concentrated solution, we conclude the diluted solution is a LHCE in which the introduced secondary solvent presents in free state and is regarded as an eligible diluent. Otherwise, the introduced secondary solvent acts as a co-solvent that coordinates to Li⁺ like the primary solvent, breaking the solution structure of the parent concentrated solution (see Fig. 1a for the experimental procedure). To demonstrate this method clearly, we take LiFSI-Methyl Propanoate (MP) system as an example and show their structural analysis process.

As shown in the Raman spectra of LiFSI-MP solutions (Fig. 1b), free-state MP molecules exhibit a C-O-C stretching vibration band centered at 850 cm⁻¹ and it shifts to 870 cm⁻¹ when MP participates in Li⁺ coordination. Simultaneously, the peak center of the vibration band of the S-N-S group of FSI⁻ shifts from 730 to 745 cm⁻¹, evidencing an enhanced interaction between FSI⁻ and Li⁺ due to the fact that more FSI⁻ anions coordinate to Li⁺ upon increasing the salt concentration. Therefore, four states of MP molecule and FSI⁻ anion can be recognized by Raman characters: “Free MP” (850 cm⁻¹), “Coord. MP” (870 cm⁻¹), “Free FSI⁻” (730 cm⁻¹), and “Coord. FSI⁻” (745 cm⁻¹), and the corresponding contents of these four states can be easily evaluated by deconvoluting the Raman peaks (see Fig. 1b).

In the same manner, we can quantitatively evaluate the solution structure for a diluted solution. Following the procedure shown in Fig. 1a, we diluted the LiFSI-2MP solution with 36 organic solvents and measured their Raman spectra (see Supplementary Fig. S1). The results can be categorized into two types: one shows almost no shift of Raman bands of both MP and FSI⁻ after introducing a secondary solvent, i.e., the contents of both Coord. MP and FSI⁻ keep more than 75%, e.g., diluting with DCB in Fig. 1b; the other one shows a significant shift of Raman bands of both MP and FSI⁻ and the reduction of the contents of both Coord. MP and FSI⁻, e.g., diluting the LiFSI-2MP solution with 8 equiv. THF results in 75% of MP and 85% of FSI⁻ changing from the coordinated state to the free state. Thereby, THF is a co-solvent for the LiFSI-2MP solution while DCB is an eligible diluent.

Apart from Raman measurements, ¹H-⁷Li 2D heteronuclear overhauser effect spectroscopy (2D HOESY) was also employed to identify the local coordination environment of a solution. A strong ¹H-⁷Li cross peak represents a close distance between H and Li, and vice versa(42). As shown in Fig. 1c, a strong ¹H (MP)-⁷Li cross peak and a weak ¹H (DCB)-⁷Li cross peak can be found for the diluted solution of LiFSI-2MP-8DCB, indicating the DCB molecule stays further away from Li⁺ as compared to MP. Whereas for the diluted solution of LiFSI-2MP-8THF, both cross peaks of ¹H (MP)-⁷Li and ¹H (THF)-⁷Li are equally strong, indicating both MP and THF molecules stay close to Li⁺. The above results suggest the DCB is a diluent and the THF is a co-solvent, consistent with the Raman results. For some samples, when the introduced secondary solvents have Raman bands overlapping with the anion or the primary solvent, it is difficult to evaluate the solution structure by deconvoluting the Raman spectra. In those cases, ¹H-⁷Li 2D HOESY spectra become the main measurement to identify a diluent.

To check if as-prepared diluted concentrated electrolytes inherit advanced physicochemical and electrochemical properties of the concentrated electrolyte, we carried out compatibility tests of lithium metal and graphite electrode with the electrolytes of LiFSI-10MP, LiFSI-2MP, LiFSI-2MP-8THF and LiFSI-2MP-8DCB (Supplementary Fig. S2), respectively. As expected, the electrolyte of LiFSI-2MP-8THF, in which the local coordination structures of Li⁺ are similar to those in LiFSI-10MP, cannot stay stable with lithium metal and graphite electrode, confirming it behaves like a conventional diluent electrolyte. In contrast, the electrolyte of LiFSI-2MP-8DCB, which possesses a solution structure similar to the parent concentrated electrolyte of LiFSI-2MP, shows high compatibility with both lithium metal and graphite electrode, demonstrating that it does inherit the advanced properties of the concentrated electrolyte. Clearly, the above results prove that the localized solution structure of electrolyte is critical for its physicochemical and electrochemical properties, and it is promising to develop

cheap and high-performance LHCEs using conventionally cheap solvents as diluents. Therefore, it is urgent to find out the rule for screening appropriate diluents for LHCEs.

Solution structure dependence: ϵ vs μ vs DN

In previous reports, the solvation structure of lithium electrolyte is usually associated with the dielectric constant of the solvent. This belief could be traced back to the studies on the classical electrolyte of 1 M LiPF₆-EC-DMC, in which the two solvents of EC and DMC have a large difference in ϵ (90.8 vs 3.09) but comparable DN values (16.4 vs 15.2). It is well known, the EC component contributes to a key solid-state electrolyte interphase that is essential for the reversible Li-intercalation/deintercalation of the graphite anode. This EC-derived interphase Chemistry is usually associated to the formation of EC-Li⁺ solvation; high- ϵ of EC is regarded as the key factor responsible for such a coordination preference for EC over DMC to Li⁺ (43-45). Accordingly, it is generally believed that the dielectric constant of solvent has a great influence on the solvation structure as well as properties of solution.

To find out the key factor for preparing a LHCE, we firstly study the influence of dielectric constant on the solution structure of a diluted system of LiFSI-2MP-8[Solv.II] system. The contents of coordinated MP and FSI⁻ in the diluted solutions vs. ϵ of Solv. II were plotted in Fig. 2a and 2b, respectively. Surprisingly, we found that neither the content of coordinated MP nor FSI⁻ shows a significant correlation with $\epsilon_{\text{Solv.II}}$. For secondary solvents with $\epsilon < 6.1$ (MP), some diluted solutions have a high content of coordinated MP and FSI⁻ (> 70%), i.e., CTC ($\epsilon = 2.4$) and PhM ($\epsilon = 4.4$), while some samples show a low content of them (< 40%), i.e., DOA ($\epsilon = 2.2$) and DEC ($\epsilon = 2.8$). Additionally, a high content of coordinated FSI⁻ remains over 90% even after introducing a high- ϵ secondary solvent such as NB ($\epsilon = 34.7$), contradicting with the common belief that a high- ϵ solvent can strongly coordinate to Li⁺ and dissociate the lithium salts. Therefore, the dielectric constant of solvents, though being a widely used descriptor for electrolyte design, does not serve as a useful screening criterion for diluents of LHCEs.

Similarly, μ of Solv. II does not show a meaningful correlation with the solution structure of the diluted solutions either (see Fig. 2c,d), whereas, DN of Solv. II shows a strong correlation with the solution structure of the diluted solutions. From Fig. 2e,f, a clear boundary separating diluents and co-solvents (referred to as “diluent boundary” hereinafter) can be observed in the LiFSI-2MP-8[Solv.II] system: for secondary solvents with DN ≤ 9 (PhM), the contents of coordinated MP and FSI⁻ remain > 70% of those in the parent LiFSI-2MP concentrated solution after diluting, indicating these secondary solvents are eligible diluents, whereas for DN ≥ 13

(BN), the contents of coordinated MP and FSI⁻ sharply decrease to < 40%, indicating that these secondary solvents act as co-solvents and the solution after diluting becomes a conventional dilute solution without a LHCE structural feature. It is noteworthy that the secondary solvents studied in this work include ethers, esters, nitriles, alcohols, aromatics and alkanes, suggesting that the above finding is insensitive to functional groups of organic solvents. Thereby, the coordination structure of the diluted solution is associated with DN of the secondary solvents rather than ϵ and μ .

General rule for screening diluent for LHCEs

The above results were obtained based on the system of LiFSI-2MP-8[Solv.II] that used MP as the primary solvent. In a diluted concentrated electrolyte, the primary solvent molecule, the secondary solvent molecule, and the anion all can possibly participate in the coordination to Li⁺. Therefore, we further investigated the impacts of the primary solvent and the salt anion on the solution structures.

To study the effects of different primary solvents on the diluent boundary, eight other solvents with DN values over 14 ~ 30 were selected as the primary solvent for the diluted systems of LiFSI-2[Solv.I]-8[Solv.II]. The solvents with DN < 11 were not used as the primary solvent because they cannot dissolve the LiFSI salt at all (see Table 1). For all the nine concentrated solutions of LiFSI-2[Solv.I] (including LiFSI-2MP), the introduction of Solv.II led to either homogenous solutions (miscible) or stratification (partial- or non-miscible). Figure 3a summarizes the results of all the 324 diluted samples. The values shown in the chart of Fig. 3 are the actual equivalent molar ratios of Solv.II dissolved in the parent LiFSI-2[Solv.I] solutions. For a value of < 0.5 (too low solubility), the sample is regarded as an immiscible solution and does not undergo any further study. Otherwise, the sample undergoes Raman and/or NMR measurements for solution structure characterizations (Supplementary Figs. S3-S10). One might expect a secondary solvent with a DN value smaller than that of the primary solvent would be a diluent, thus leading to a varied diluent boundary determined by the primary solvent. Surprisingly, Figure 3a shows all the nine systems of LiFSI-2[Solv.I]-8[Solv.II] have the same diluent boundary: the diluted samples keep LHCE structures when DN \leq 10 but become conventional dilute solutions when DN > 13.

We then studied the effects of salt-anions on the diluent boundary. Five lithium salts (LiX) with different dissociation abilities, including LiFSI, lithium hexafluorophosphate (LiPF₆), lithium tetrafluoroborate (LiBF₄), bis(trifluoromethylsulphonyl)imide (LiTFSI), and lithium

triflate (LiOTf), were selected for a comparison study. Using MP as the primary solvent and 36 secondary solvents mentioned above, we prepared 180 diluted solutions of LiX-2MP-8[Solv.II] and analyzed their coordination structures (Supplementary Figs. S11-S14). The results are summarized in Fig. 3b. Clearly, it shows that regardless the anion type, the diluent boundary is fixed at $DN = \sim 10$. From these results, we generalize three features regarding the diluent boundary: I) it has a DN value smaller than that of the primary solvent; II) it is fixed at $DN = \sim 10$, independent of the types of primary solvents investigated here; III) it is insensitive to the anions of the Li-salts. Hence, supported by a thorough investigations involving ~ 500 samples, we identified a simple and general rule for screening a diluent for LHCEs: an eligible diluent must have a DN with the value of no more than 10, independent of the types of organic solvents or salt anions.

Mechanistic understanding of DN-based design principle

To understand the origin of the diluent boundary, we explored the solution structures of a few representative electrolytes via *ab initio* molecular dynamic simulations (AIMD, see computational details in Supplementary Experimental). Here we focus on LiFSI-2MP-2THF and LiFSI-2MP-2PhH as the DN of THF (28) is significantly different from that of PhH (0.1) while they have comparable dielectric constants ($\epsilon_{\text{THF}} = 8$ and $\epsilon_{\text{PhH}} = 2.3$). The AIMD snapshots of typical local environments of Li^+ in these two electrolytes reveal that all low-DN PhH molecules remain as free-state solvents, whereas nearly all high-DN THF molecules participate in the coordination to Li^+ . This is further confirmed by the calculated radial distribution functions (RDFs) for the pairs of Li^+ and secondary solvent molecules. As shown in Fig. 4a, the RDF of Li^+ -THF has a pronounced peak at 2 Å, an indicator of strong interactions. On the contrary, the RDFs of Li^+ -PhH are largely featureless, suggesting PhH molecules homogeneously distribute in solution. We carried out additional modeling using Li-salts of different anions (e.g., TFSI⁻, BF₄⁻, and OTf⁻), and the obtained RDFs (see Supplementary Fig. S15) all showed that the low-DN PhH is a diluent and the high-DN THF is a co-solvent regardless the anion type, in agreement with experimental observations.

The solution structures revealed from AIMD hint that the DN value of Solv.II could be correlated with their coordination strength to Li^+ . Based on the local environments of Li^+ identified from AIMD, we propose to use the interaction energy defined as $\Delta E = \frac{1}{2}\{E[\text{LiX} \cdots 2\text{Solv. II}] - E[\text{LiX}] - 2E[\text{Solv. II}]\}$ to gauge the coordination ability of Solv.II, where $E[\text{LiX} \cdots 2\text{Solv. II}]$ is the energy of a molecular complex consisted of a Li^+ , an anion (X

= FSI⁻ and TFSI⁻), and two coordinated Solv.II molecules (see inset in Fig. 4b), $E[\text{LiX}]$ is the energy of an isolated anion-cation pair, and $E[\text{Solv.II}]$ is the energy of an isolated Solv.II molecules. As shown in Fig. 4b, ΔE is almost linearly dependent on DN, supporting that DN is a good descriptor of the coordination ability. Moreover, for the same Solv.II molecule, the values of ΔE are insensitive to the types of anions (FSI⁻ and TFSI⁻). Such anion-independence of ΔE can be understood as follows. The Li⁺-anion interaction is mostly of the electrostatic (ionic) nature that the anion completely takes the 2s electron from the Li. In contrast, the interaction between Li⁺ and a solvent molecule is a typical donor-acceptor coordination involving the lone pair of electrons from the solvent (e.g., O) and the empty 2s-orbital of Li⁺. As Li⁺ has highly concentrated charge, the energy of the 2s orbital is dictated by the Li⁺ core (nucleus plus 1s electrons) while less impacted by nearby anions, likely leading to an anion-independent Li⁺-solvent interaction. We also computed the differential charge densities of LiFSI-2THF and LiTFSI-2THF molecular complexes (Fig. 4b inset), evidencing charge accumulations between Li⁺ and solvent molecules and the electron sharing nature of the coordination. Notably, the two molecular complexes exhibit nearly identical differential charge density isosurfaces of the same value. Altogether, quantum mechanical calculations confirm that DN serves as a reliable and general measurement of the coordination ability of solvents to Li⁺ universal for various Li-salts.

On the other hand, the failure of the ϵ -based design principle for LHCEs can be understood from the localized structural point view. The interaction between two charged ions separated by a distance r is described by the Coulomb law: $F = z_1 z_2 e^2 / 4\pi\epsilon_0 \epsilon r^2$, where z_1 and z_2 are the charges of the ions, respectively, ϵ_0 is the vacuum permittivity, and ϵ is the dielectric constant of the medium relative to vacuum. Apparently, in a dilute homogenous solution with a high- ϵ solvent, ions would have a high probability of staying free at a given salt concentration and ion association would be less likely to occur due to the weaker Coulomb interactions. However, such dielectric continuum solvation model is not applicable to salt-concentrated electrolytes, in which Li⁺ cations, anions, and solvent molecules are strongly bounded locally at the molecular level. It is the local interactions between salt ions and solvents that dictate the local solution structure, whereas the solvent can no longer be considered as a dielectric continuum. Because DN is a good descriptor of the solvent coordination strength to Li⁺, it is reasonable that the DN value is a more relevant solvent parameter to realize LHCEs.

Atomistic model of LHCE for diluent design

Based on the combined experimental and theoretical results, we now propose a general atomistic model of LHCE. The LHCE can be understood as primary-solvent-coordinated localized Li-salt clusters embedded in free-state secondary solvents. The Li-salt clusters are consisted of positively and negatively charged units of Solv.I-Li⁺-anion pairs. This atomistic model allows for a heuristic explanation to the emergence of a universal DN-based diluent selection rule and the intriguing features of diluent boundary. As shown in Fig. 4c, the free energies of two solution structures, localized concentrated solution and conventional dilute solution, depend on the DN of the secondary solvent, and the former is favored in low-DN solvents whereas the latter is favored in high-DN solvents. This gives rise to a solution structure transition at a critical DN that defines the diluent boundary. Such transition can be considered as a re-dissolution process: the localized Li-salt clusters dissolve in a secondary solvent. Therefore, the critical DN value is intrinsically determined by the minimum interaction strength (ΔE_c) needed to dissolve the localized Li-salt clusters consisted of Solv.I-Li⁺-anion pairs. Given that a defining feature of a primary solvent is its ability to dissolve the Li-salts, we argue that the Li⁺-Solv.I interactions within the clusters are already rather strong; the re-dissolution is mainly achieved through Li⁺-Solv.II interactions that break the Li⁺-anion pairs. Therefore, the magnitude of ΔE_c , mostly due to the Li⁺-anion interaction, does not depend on the primary solvent type (feature II). The re-dissolution would occur when the coordination strength of Solv. II to Li⁺, gauged by the DN value, is stronger than ΔE_c , thus explaining the observation that the diluent should have a DN smaller than that of the primary solvent (feature I). Experimental results reveal a weak anion-dependence of ΔE_c , which might appear surprising at first sight. But our quantum mechanical calculations already showed that the Li⁺-Solv.II interaction is rather anion-insensitive, supporting the hypothesis that the local Li⁺-anion interaction is of the electrostatic nature and remains nearly constant for anions of the same charge (-1) (feature III). It is reasonable to conclude that ΔE_c , in the unit of DN value, is ~ 10 . In summary, our model with justified anion-insensitive critical interaction strength for re-dissolution offers straightforward explanations to all three features of diluent boundary.

Within this model picture, we can further deduce that a secondary solvent that cannot dissolve the Li-salt is a dilute, otherwise it is a co-solvent. This solubility-based selection rule, if valid, not only supports the proposed atomistic model but also serves as a convenient diluent design principle. We thus carried out dissolution experiments to check this prediction.

Solubility-based selection rule

We first tested the solubility of LiFSI salt in various organic solvents. The saturated mole fractions of LiFSI (X_{LiFSI}) were listed in Table 1. X_{LiFSI} vs DN was plotted in Fig. 5a. Obviously, the X_{LiFSI} value dramatically decreases by almost two orders when the DN value of organic solvents becomes smaller than 11, demonstrating a clear Li-salt dissolving boundary with the same DN position as that of the diluent boundary as shown in Fig. 3. Whereas no meaningful correlation can be found between X_{LiFSI} and ϵ or μ of solvents (see Fig. 5b,c). Accordingly, the coincidence between the salt dissolving boundary and the diluent boundary can provide a facile method to screen the diluent for LHCEs. To quick verify the universality of this salt dissolving boundary, we carried out another 180 dissolution measurements by mixing five lithium salts with 36 organic solvents in a small salt-to-solvent molar ratio of 1:50. If the small amount of lithium salt cannot fully dissolve in the solvent to form a homogenous solution, we regard the salt is insoluble in the solvent (marked in white), otherwise we regard the salt is soluble in the solvent (marked in orange). As shown in Fig. 5d, all the five salts have nearly identical dissolving boundary at $\text{DN} = \sim 10$ insensitive to the anion type, confirming the validity of solubility-based selection rule as well as the robustness of proposed atomistic LHCE model.

It is noteworthy that although DN demonstrates as a reliable parameter to determine the salt dissolving boundary, i.e., the solvent must have $\text{DN} > 10$ to dissolve a lithium salt, it does not mean a solvent with a larger DN has a higher solubility. As shown in Fig. 5a, no clear tendency between X_{LiFSI} and DN can be found in the region of $\text{DN} > 10$. Hence, based on our study of a large number of samples, we would also like to point out that some common beliefs of “high-DN (or high-polarity or high- ϵ) solvents promote the solubility of salts” are actually inaccurate and misleading(46-49). In fact, the salt dissolution process involves complicated physical and Chemical changes, and many possible factors, such as lattice energy, van der Waal’s forces, and steric factors, could affect it(50).

Conclusions

Structural studies on hundreds of electrolytes reveal that the dielectric constant or polarity of a solvent is not a useful parameter to design the LHCEs that are in nanoscale inhomogeneity. Instead, the DN, serving as a robust descriptor for LHCEs design, can be used to screen dilutes: to achieve LHCE structure, the primary solvent must have $\text{DN} > 10$ and the diluent must have $\text{DN} \leq 10$. The diluent boundary is fixed at $\text{DN} \approx 10$, independent of the type of primary solvents and salt anions. These intriguing features can be explained with an atomistic model of LHCE,

in which primary-solvent-coordinated Li-salt clusters are embedded in free-state secondary solvents, and the local solution structure is dictated by the interaction strength between the secondary solvent and Li^+ that can be gauged by the DN of secondary solvent. When the DN increases to a critical DN of ~ 10 , a transition of local solution structure occurs from the heterogeneous LHCE to conventional homogeneous dilute solution. Such transition can be understood as a re-dissolution process of the primary-solvent-coordinated Li-salt clusters in the secondary solvents, naturally leading to a simpler solubility-based design principle that is beneficial for a rapid screening of solvents for diluents: Li-salt-insoluble solvents are diluents while Li-salt-soluble solvents become co-solvents. Both the DN- and solubility-based screening rules are expected to be applicable to other electrolytes systems.

Acknowledgement

This work was supported by Westlake Education Foundation, National Natural Science Foundation of China (Grant No. 21975207), Zhejiang Provincial Natural Science Foundation of China (Grant No. LQ21B030006), and Postdoctoral Science Foundation of Zhejiang Province (Grant No. ZJ2020079). The calculations and NMR measurements were performed at Westlake HPC Center and Instrumentation and Service Center for Molecular Sciences, respectively. The authors thank Prof. Wenjie Dai for his useful suggestions on the manuscript and Dr. Xiaohuo Shi for his assistance in NMR data interpretation.

Author contributions

J.W. and J.C. designed the experiments. J.C. and H.Z. carried out the experiments. S.L. directed the computation. S.L. and C.K. designed and performed the DFT-MD simulations. All authors contributed to the discussion and the manuscript preparation. J.C., H.Z. and C.K. contributed equally to this work. J.W. conceived and led the project.

Competing interests

The authors declare no competing financial interests.

Supporting Information Available: Experimental details, computational details, Raman spectra, compatibility of lithium metal and graphite electrodes in the electrolytes, and calculated RDFs are included in the Supplementary Information.

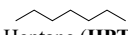
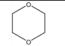
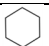
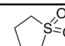
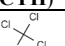
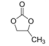
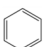
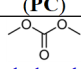
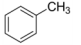
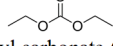
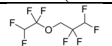
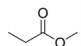
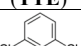
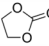
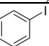
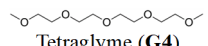
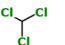
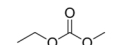
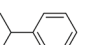
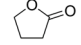
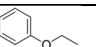
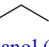
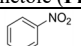
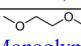
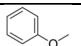
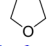
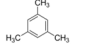
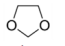
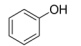
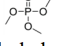
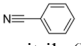
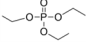
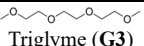

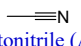
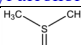
References

- 1 Xu, K. Nonaqueous liquid electrolytes for lithium-based rechargeable batteries. *Chem. Rev.* **104**, 4303-4417 (2004).
- 2 Xu, K. Electrolytes and interphases in Li-ion batteries and beyond. *Chem. Rev.* **114**, 11503-11618 (2014).
- 3 Yamada, Y. & Yamada, A. Review—Superconcentrated Electrolytes for Lithium Batteries. *J. Electrochem. Soc.* **162**, A2406-A2423 (2015).
- 4 Zheng, J. M., Lochala, J. A., Kwok, A., Deng, Z. Q. D. & Xiao, J. Research Progress towards Understanding the Unique Interfaces between Concentrated Electrolytes and Electrodes for Energy Storage Applications. *Adv. Sci.* **4**, 1700032 (2017).
- 5 Yamada, Y., Wang, J., Ko, S., Watanabe, E. & Yamada, A. Advances and issues in developing salt-concentrated battery electrolytes. *Nat. Energy* **4**, 269-280 (2019).
- 6 Borodin, O., Self, J., Persson, K. A., Wang, C. S. & Xu, K. Uncharted Waters: Super-Concentrated Electrolytes. *Joule* **4**, 69-100 (2020).
- 7 Jeong, S. K., Inaba, M., Iriyama, Y., Abe, T. & Ogumi, Z. Electrochemical intercalation of lithium ion within graphite from propylene carbonate solutions. *Electrochem. Solid State Lett.* **6**, A13-A15 (2003).
- 8 Yoshida, K. *et al.* Oxidative-stability enhancement and charge transport mechanism in glyme-lithium salt equimolar complexes. *J. Am. Chem. Soc.* **133**, 13121-13129 (2011).
- 9 Yamada, Y. *et al.* Unusual stability of acetonitrile-based superconcentrated electrolytes for fast-charging lithium-ion batteries. *J. Am. Chem. Soc.* **136**, 5039-5046 (2014).
- 10 Suo, L. M. *et al.* "Water-in-salt" electrolyte enables high-voltage aqueous lithium-ion chemistries. *Science* **350**, 938-943 (2015).
- 11 Wang, J. *et al.* Superconcentrated electrolytes for a high-voltage lithium-ion battery. *Nat. Commun.* **7**, 12032 (2016).
- 12 Wang, J. H. *et al.* Fire-extinguishing organic electrolytes for safe batteries. *Nat. Energy* **3**, 22-29 (2018).
- 13 Zeng, Z. Q. *et al.* Non-flammable electrolytes with high salt-to-solvent ratios for Li-ion and Li-metal batteries. *Nat. Energy* **3**, 674-681 (2018).
- 14 Alvarado, J. *et al.* A carbonate-free, sulfone-based electrolyte for high-voltage Li-ion batteries. *Mater. Today* **21**, 341-353 (2018).
- 15 Ko, S., Yamada, Y. & Yamada, A. An overlooked issue for high-voltage Li-ion batteries: Suppressing the intercalation of anions into conductive carbon. *Joule* **5**, 998-1009 (2021).
- 16 Suo, L. M., Hu, Y. S., Li, H., Armand, M. & Chen, L. Q. A new class of Solvent-in-Salt electrolyte for high-energy rechargeable metallic lithium batteries. *Nat. Commun.* **4**, 1481 (2013).
- 17 Qian, J. F. *et al.* High rate and stable cycling of lithium metal anode. *Nat. Commun.* **6**, 6362 (2015).
- 18 Suo, L. M. *et al.* Fluorine-donating electrolytes enable highly reversible 5-V-class Li metal batteries. *Proc. Natl. Acad. Sci. USA* **115**, 1156-1161 (2018).
- 19 Fan, X. L. *et al.* Highly Fluorinated Interphases Enable High-Voltage Li-Metal Batteries. *Chem* **4**, 174-185 (2018).
- 20 Dokko, K. *et al.* Solvate Ionic Liquid Electrolyte for Li-S Batteries. *J. Electrochem. Soc.* **160**, A1304-A1310 (2013).
- 21 Pang, Q. *et al.* Tuning the electrolyte network structure to invoke quasi-solid state sulfur conversion and

- suppress lithium dendrite formation in Li-S batteries. *Nat. Energy* **3**, 783-791 (2018).
- 22 Liu, T. *et al.* Ultralight Electrolyte for High-Energy Lithium-Sulfur Pouch Cells. *Angew. Chem. Int. Ed.* **60**, 17547-17555 (2021).
- 23 Ren, X. D. *et al.* Localized High-Concentration Sulfone Electrolytes for High-Efficiency Lithium-Metal Batteries. *Chem* **4**, 1877-1892 (2018).
- 24 Cao, X. *et al.* Monolithic solid-electrolyte interphases formed in fluorinated orthoformate-based electrolytes minimize Li depletion and pulverization. *Nat. Energy* **4**, 796-805 (2019).
- 25 Fan, X. L. *et al.* All-temperature batteries enabled by fluorinated electrolytes with non-polar solvents. *Nat. Energy* **4**, 882-890 (2019).
- 26 Piao, N. *et al.* Countersolvent Electrolytes for Lithium-Metal Batteries. *Adv. Energy Mater.* **10**, 1903568 (2020).
- 27 Doi, T., Shimizu, Y., Hashinokuchi, M. & Inaba, M. Dilution of Highly Concentrated LiBF₄/Propylene Carbonate Electrolyte Solution with Fluoroalkyl Ethers for 5-V LiNi_{0.5}Mn_{1.5}O₄ Positive Electrodes. *J. Electrochem. Soc.* **164**, A6412-A6416 (2017).
- 28 Takada, K., Yamada, Y. & Yamada, A. Optimized Nonflammable Concentrated Electrolytes by Introducing a Low-Dielectric Diluent. *ACS Appl. Mater. Interfaces* **11**, 35770-35776 (2019).
- 29 Jia, H. P. *et al.* High-Performance Silicon Anodes Enabled By Nonflammable Localized High-Concentration Electrolytes. *Adv. Energy Mater.* **9**, 1900784 (2019).
- 30 Zhang, X. *et al.* Advanced Electrolytes for Fast - Charging High - Voltage Lithium - Ion Batteries in Wide - Temperature Range. *Adv. Energy Mater.* **10**, 2000368 (2020).
- 31 Christian Reichardt, T. W. *Solvents and Solvent Effects in Organic Chemistry* (Fourth, Updated and Expanded Edition). (2010).
- 32 Bogle, X., Vazquez, R., Greenbaum, S., Cresce, A. & Xu, K. Understanding Li(+)-Solvent Interaction in Nonaqueous Carbonate Electrolytes with (17)O NMR. *J. Phys. Chem. Lett.* **4**, 1664-1668 (2013).
- 33 Yao, N. *et al.* An Atomic Insight into the Chemical Origin and Variation of the Dielectric Constant in Liquid Electrolytes. *Angew. Chem. Int. Ed.* **60**, 21473-21478 (2021).
- 34 Ding, J. F. *et al.* Non-Solvating and Low-Dielectricity Cosolvent for Anion-Derived Solid Electrolyte Interphases in Lithium Metal Batteries. *Angew. Chem. Int. Ed.* **60**, 11442-11447 (2021).
- 35 Jia, H. *et al.* Toward the Practical Use of Cobalt-Free Lithium-Ion Batteries by an Advanced Ether-Based Electrolyte. *ACS Appl. Mater. Interfaces* **13**, 44339-44347 (2021).
- 36 Wu, Q. *et al.* Enhancing the Cycling Stability for Lithium-Metal Batteries by Localized High-Concentration Electrolytes with 2-Fluoropyridine Additive. *ACS Appl. Energy Mater.* **4**, 10234-10243 (2021).
- 37 Pham, T. D. & Lee, K. K. Simultaneous Stabilization of the Solid/Cathode Electrolyte Interface in Lithium Metal Batteries by a New Weakly Solvating Electrolyte. *Small* **17**, 2100133 (2021).
- 38 Ueno, K. *et al.* Li⁺ Solvation and Ionic Transport in Lithium Solvate Ionic Liquids Diluted by Molecular Solvents. *J. Phys. Chem. C* **120**, 15792-15802 (2016).
- 39 Zheng, J. M. *et al.* Extremely Stable Sodium Metal Batteries Enabled by Localized High-Concentration Electrolytes. *ACS Energy Lett.* **3**, 315-321 (2018).
- 40 Zheng, J. *et al.* High - Fluorinated Electrolytes for Li - S Batteries. *Adv. Energy Mater.* **9**, 1803774 (2019).

- 41 He, M. X. *et al.* Realizing Solid-Phase Reaction in Li-S Batteries via Localized High-Concentration Carbonate Electrolyte. *Adv. Energy Mater.* **11**, 2101004 (2021).
- 42 Singh, S., Nanda, R. & Dorai, K. Structural and dynamical aspects of PEG/LiClO₄ in solvent mixtures via NMR spectroscopy. *Magn. Reson. Chem.* **57**, 412-422 (2019).
- 43 Masayuki Morita, Y. A., Nobuko Yoshimoto and Masashi Ishikawa. A Raman spectroscopic study of organic electrolyte solutions based on binary solvent systems of ethylene carbonate with low viscosity solvents which dissolve different lithium salts. *J. Chem. Soc. Faraday Trans.* **94**, 3451-3456 (1998).
- 44 Xu, K., Lam, Y. F., Zhang, S. S., Jow, T. R. & Curtis, T. B. Solvation sheath of Li⁺ in nonaqueous electrolytes and its implication of graphite/electrolyte interface chemistry. *J. Phys. Chem. C* **111**, 7411-7421 (2007).
- 45 Yang, L., Xiao, A. & Lucht, B. L. Investigation of solvation in lithium ion battery electrolytes by NMR spectroscopy. *J. Mol. Liq.* **154**, 131-133 (2010).
- 46 Johnson, L. *et al.* The role of LiO₂ solubility in O₂ reduction in aprotic solvents and its consequences for Li-O₂ batteries. *Nat. Chem.* **6**, 1091-1099 (2014).
- 47 Gupta, A., Bhargav, A. & Manthiram, A. Highly Solvating Electrolytes for Lithium-Sulfur Batteries. *Adv. Energy Mater.* **9**, 1803096 (2019).
- 48 Baek, M., Shin, H., Char, K. & Choi, J. W. New High Donor Electrolyte for Lithium-Sulfur Batteries. *Adv. Mater.* **32**, e2005022 (2020).
- 49 Xin, N., Sun, Y. J., He, M. G., Radke, C. J. & Prausnitz, J. M. Solubilities of six lithium salts in five non-aqueous solvents and in a few of their binary mixtures. *Fluid Phase Equilib.* **461**, 1-7 (2018).
- 50 Gutmann, V. *Coordination Chemistry in Non-Aqueous Solutions*. (Springer-Verlag Wien, 1968).

Table 1. Information about the studied organic solvents: DN values, dielectric constants, dipole moments, and their saturated solutions with LiFSI salt.

Label	Solvents	DN	ϵ	μ	X_{LiFSI}^*	Label	Solvents	DN	ϵ	μ	X_{LiFSI}^*
1	 Heptane (HPT)	0.0	1.9	0	1.51E-05	19	 1,4-Dioxane (DOA)	14.8	2.2	0.45	0.15
2	 Cyclohexane (CYH)	0.0	2.0	0	4.38E-05	20	 Tetramethylene sulfone (SL)	14.8	42.0	4.68	0.30
3	 Tetrachloromethane (CTC)	0.0	2.4	0	6.18E-06	21	 Propylene carbonate (PC)	15.1	64.6	4.94	0.43
4	 Benzene (PhH)	0.1	2.3	0	4.08E-05	22	 Dimethyl carbonate (DMC)	15.2	3.0	0.93	0.48
5	 Toluene (TOL)	0.1	2.4	0.31	4.81E-05	23	 Diethyl carbonate (DEC)	16.0	2.8	1.07	0.49
6	 Hydrofluoroether (TTE)	1.9	6.2	-	9.93E-04	24	 Methyl propanoate (MP)	16.2	6.1	1.67	0.45
7	 Dichlorobenzene (DCB)	2.0	4.9	1.68	2.09E-05	25	 Ethylene carbonate (EC)	16.4	90.8	4.51	0.45
8	 Iodobenzene (IB)	4.0	4.6	1.71	2.67E-05	26	 Tetraglyme (G4)	16.6	7.7	-	0.66
9	 Chloroform (TCM)	4.0	4.8	1.15	2.35E-03	27	 Ethyl Methyl Carbonate (EMC)	17.2	3.0	-	0.40
10	 Cumene (iPB)	6.0	2.4	0.65	1.72E-03	28	 γ -Butyrolactone (γ -BL)	18.0	39.0	4.27	0.51
11	 Phenetole (PhE)	8.0	4.3	1.41	1.72E-03	29	 Ethanol (ET)	19.2	24.6	1.66	0.39
12	 Nitrobenzene (NB)	8.1	34.7	4.28	1.72E-02	30	 Monoglyme (DME)	20.0	7.2	1.71	0.52
13	 Anisole (PhM)	9.0	4.4	1.36	2.84E-03	31	 Tetrahydrofuran (THF)	21.0	8.0	1.69	0.48
14	 Mesitylene (MES)	10.0	2.3	0.10	1.32E-04	32	 1,3-dioxolane (DOL)	21.2	7.3	1.19	0.05
15	 Phenol (PhOH)	11.0	12.4	1.55	0.16	33	 Trimethyl phosphate (TMP)	23.0	20.6	2.82	0.53
16	 Benzonitrile (BN)	13.0	25.7	4.28	0.44	34	 Triethyl phosphate (TEP)	23.4	13.1	2.86	0.52
17	 Triglyme (G3)	14.0	7.5	2.16	0.66	35	 n-Amyl alcohol (nAA)	25.0	13.9	1.70	0.35
18	 Acetonitrile (AN)	14.1	36.0	3.44	0.48	36	 Dimethyl sulfoxide (DMSO)	29.8	46.4	4.10	0.51

* X_{LiFSI} represents the maximum mole fraction of LiFSI in corresponding solvents.

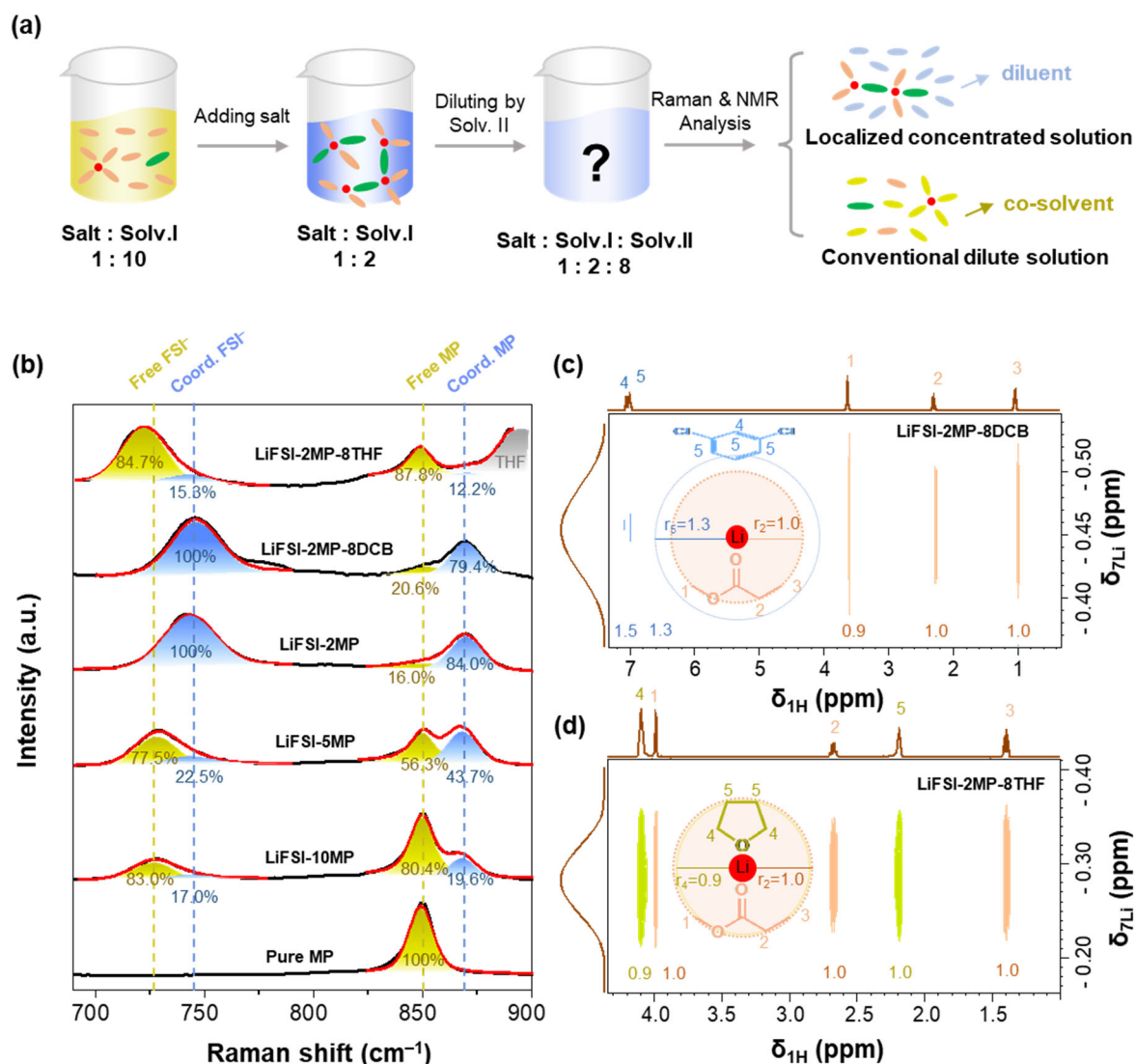


Fig. 1 | Representative demonstration of preparation and characterization of LHCEs. (a) Schematic diagram of experimental procedures for electrolyte preparation and characterization. (b) Quantitative analysis of Raman spectra of LiFSI-MP system with different salt concentrations and secondary solvents. It shows that the diluted solution of LiFSI-2MP-8DCB has a similar coordination structure with the parent concentrated solution of LiFSI-2MP, evidencing the former is a LHCE and DCB is an eligible diluent, while, the diluted solution of LiFSI-2MP-8THF has a similar coordination structure with the dilute solution of LiFSI-10MP, evidencing THF is not a diluent but a co-solvent. (c, d) are quantitative analysis of the relative distances of Li⁺-Solv.I and Li⁺-Solv.II from ¹H-⁷Li 2D HOESY NMR spectra of LiFSI-2MP-8DCB (c) and LiFSI-2MP-8THF (d). It indicates that DCB stays far away from Li⁺ and acts as a diluent while THF stays close to Li⁺ and acts as a diluent, consistent with the Raman results.

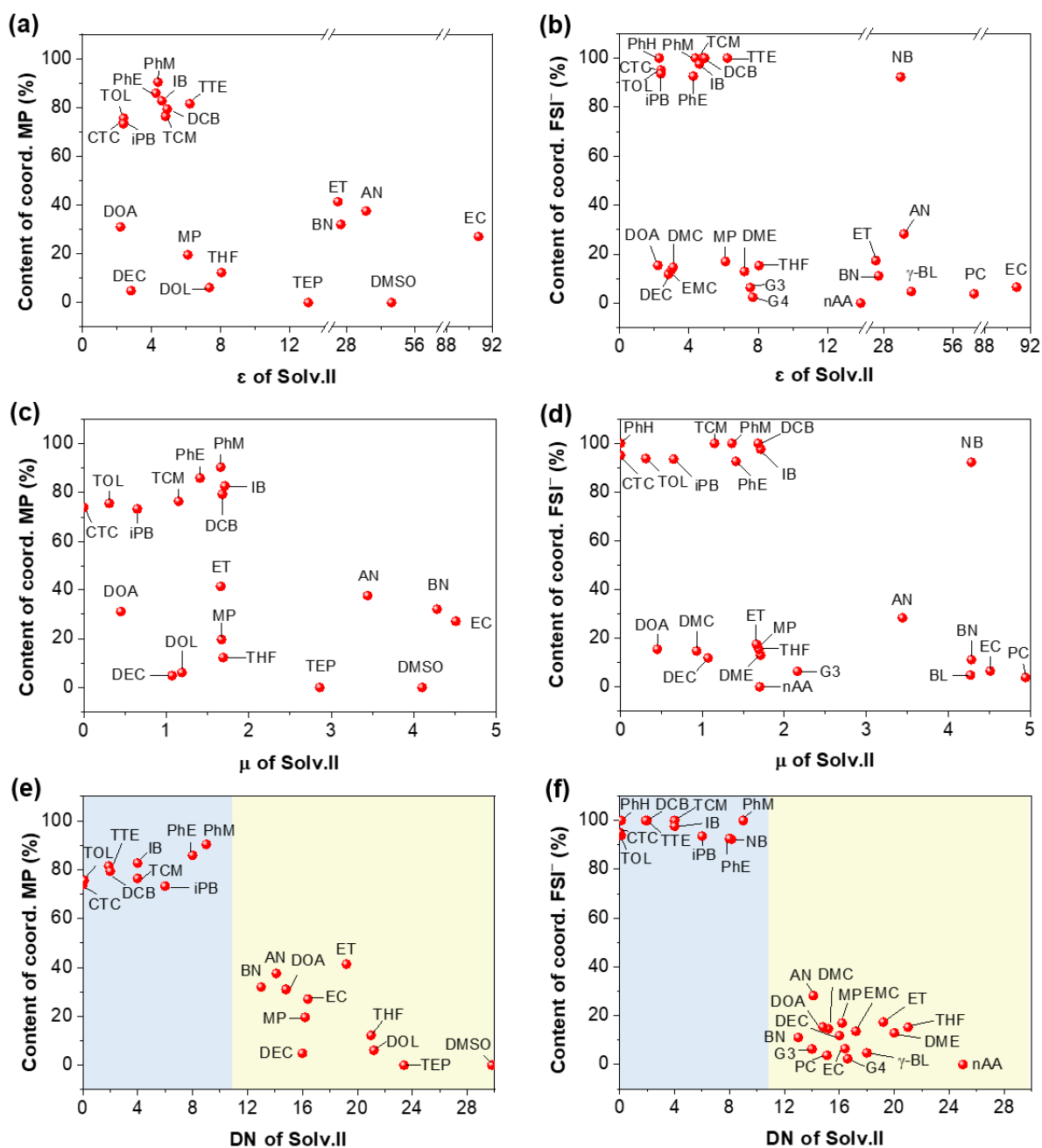


Fig. 2 | Correlation of coordinated species in the LiFSI-2MP-8[Solv.II] system with ϵ or μ or DN of secondary solvents. (a, b) show the content of coordinated MP molecules and FSI⁻ anions in the diluted solutions varying with ϵ of the introduced secondary solvents, respectively. (c, d) show the content of coordinated MP molecules and FSI⁻ anions in the diluted solutions varying with μ of the introduced secondary solvents, respectively. (e, f) show the content of coordinated MP molecules and FSI⁻ anions in the diluted solutions varying with DN of the introduced secondary solvents, respectively. No clear correlation can be found between the coordinated structure and ϵ or μ of the introduced secondary solvents. By contrast, a clear correlation can be observed between the coordinated structure and DN of the introduced secondary solvents. For some diluted solutions, because the introduced secondary solvents have Raman bands overlapping with either MP or FSI⁻, the corresponding contents of coordinated MP or FSI⁻ are difficult to evaluate and thus are not shown.

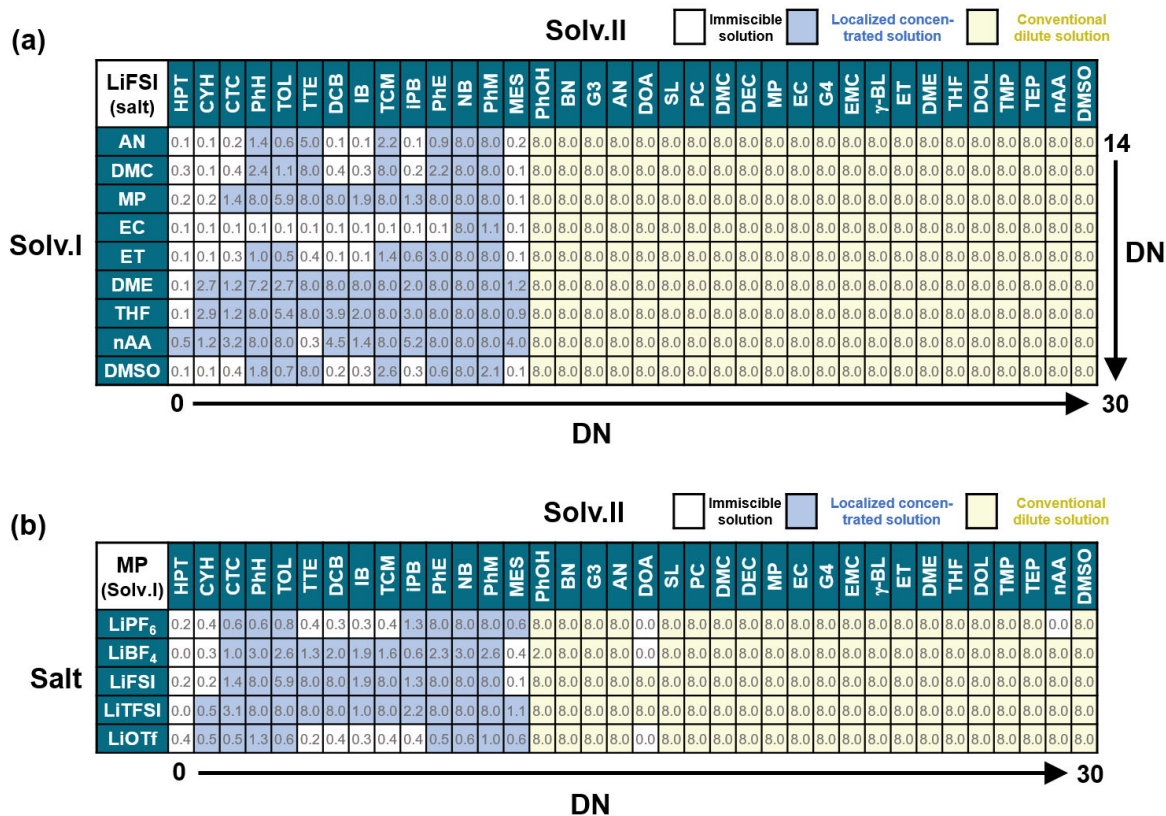


Fig. 3 | Coordination structures of the diluted concentrated electrolytes dependent on primary and secondary solvents as well as lithium salts. (a) Coordination structures of the LiFSI-2[Solv.I]-8[Solv.II] system dependent on primary and secondary solvents. (b) Coordination structures of the [LiX]-2MP-8[Solv.II] system dependent on lithium salts. In some cases, the introduction of secondary solvent leads to the solution stratification. The values shown in the chart are the real equivalent molar ratio of secondary solvents dissolved in the parent concentrated solution. A diluted solution with a too low content of secondary solvent (<0.5) is regarded as an immiscible solution (marked in white); that with a localized concentrated structure is marked in blue; the others with conventional dilute solution (marked in orange). For all the studied diluted solutions, the localized concentrated structure of the parent concentrated solution can be preserved only if DN of the introduced secondary solvent is less than that of 10. This rule is valid for all the 504 diluted samples of [LiX]-2[Solv.I]-8[Solv.II], indicating it independent of primary and secondary solvents and anions.

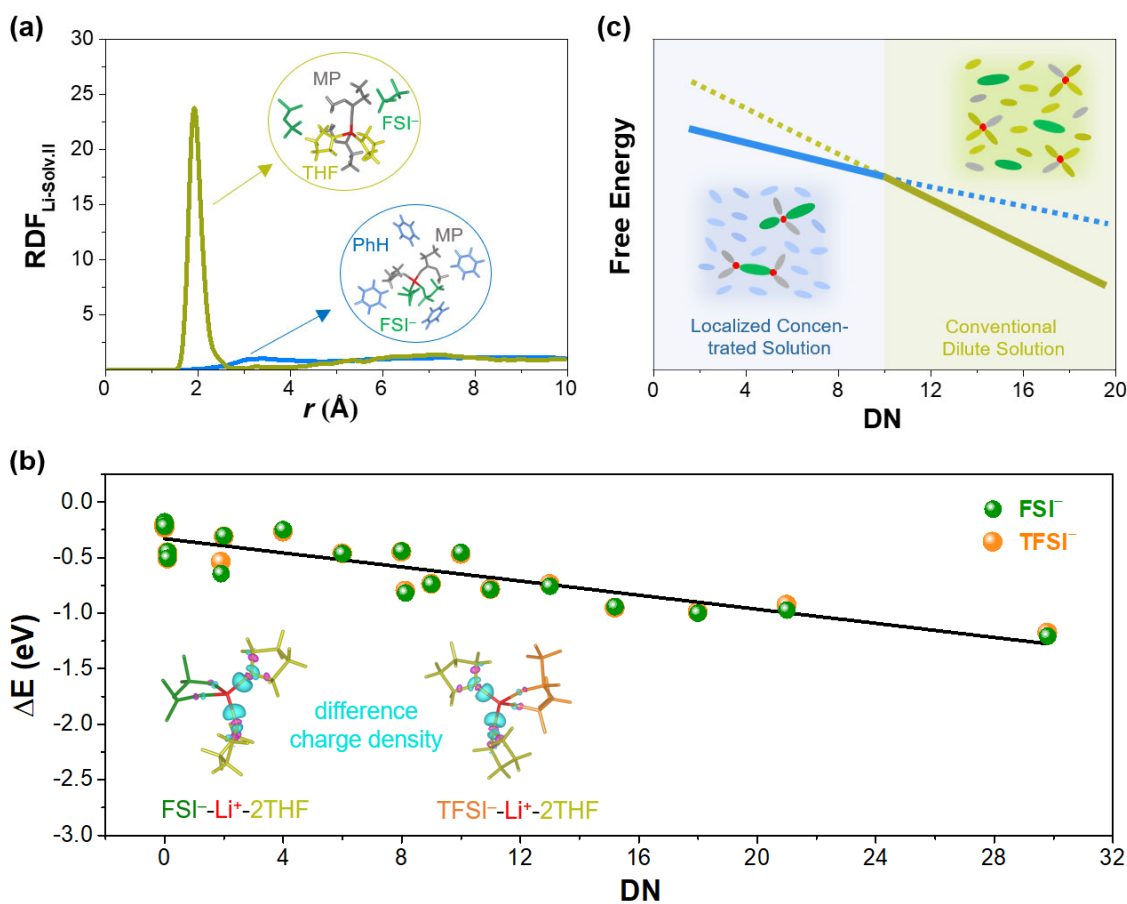


Fig. 4 | Quantum mechanical explanation of DN-based LHCE design principle. (a) Comparison of radial distribution functions (RDFs) of Li-Solv.II pairs and typical local coordination environment of Li⁺ in LiTFSI-2MP-2PhH and LiTFSI-2MP-2THF electrolytes from *ab initio* molecular dynamic simulations. (b) Linear scaling relationship between coordination energy ΔE of Solv. II with Li and DN values computed with density functional theory. (c) Schematic diagram of proposed solution structure transition in dilute electrolytes using the DN value of secondary solvent as the collective variable of free energy.

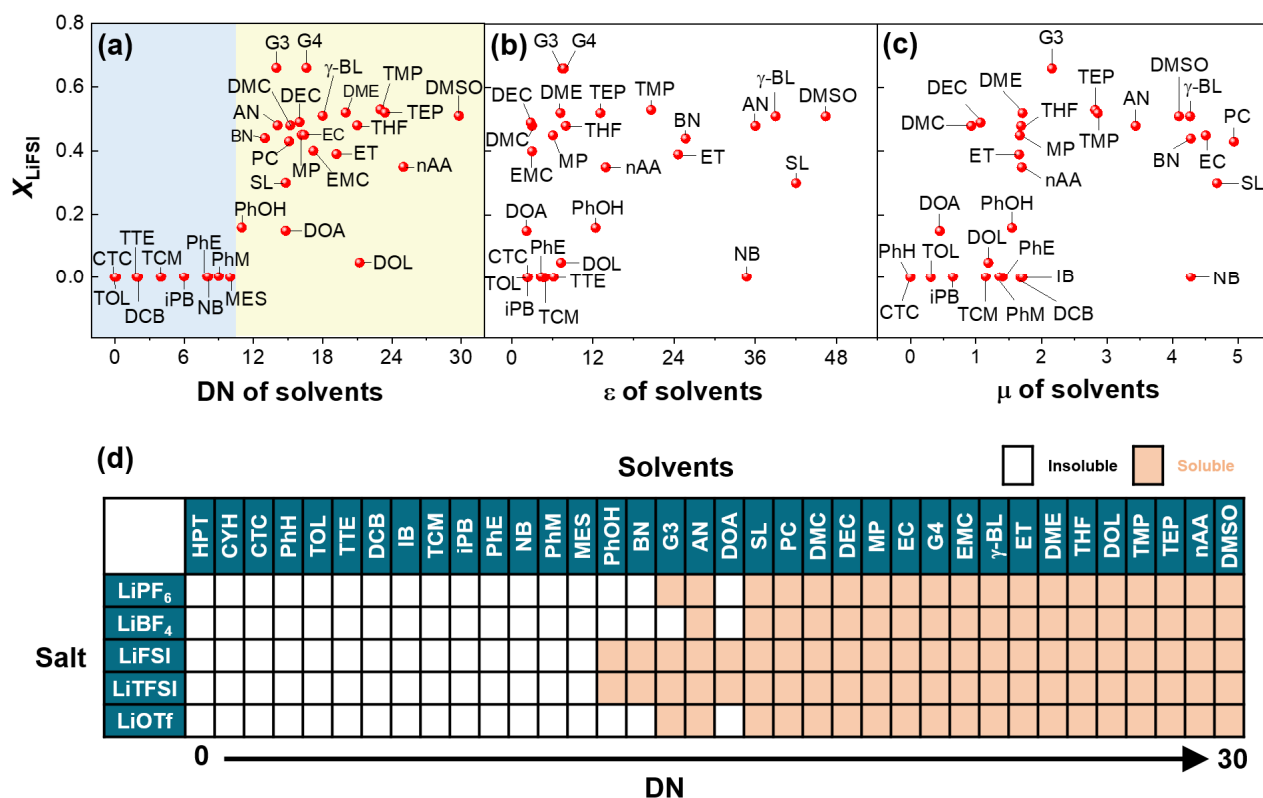


Fig. 5 | Lithium salts dissolving in various organic solvents. (a-c) show the maximum mole fractions of LiFSI salt dissolving in the solvents with different DN, ϵ , and μ , respectively. A clear correlation can be only observed between X_{LiFSI} and DN of the solvents. (d) Solubility test of five lithium salts in different organic solvents. Each lithium salt was introduced in 36 organic solvents in a small salt-to-solvent molar ratio of 1 : 50, respectively. If this small amount of lithium salt cannot fully dissolve in the solvent to form a homogenous solution, we regard the salt is insoluble in the solvent (marked in white), otherwise we regard the salt is soluble in the solvent (marked in orange). The Li-salt dissolving boundary locates at DN = ~10, which is almost the same with the diluent boundary for LHCEs (shown in Fig. 3), indicating the salt dissolving test could be used as a simple yet efficient way to the rapid search of appropriate diluents for salt-concentrated electrolytes.

Supplementary Information

Design localized high concentration electrolytes via donor number and solubility

Juner Chen,^{1,2,6} Han Zhang,^{1,3,6} Changming Ke,^{4,5,6} Shi Liu,^{4,5*} Jianhui Wang^{1,2,3*}

1 Key Laboratory of 3D Micro/Nano Fabrication and Characterization of Zhejiang Province,

School of Engineering, Westlake University, Hangzhou, China

2 Institute of Advanced Technology, Westlake Institute for Advanced Study, Hangzhou, China

3 Department of Chemistry, Zhejiang University, Hangzhou, China

4 Key Laboratory for Quantum Materials of Zhejiang Province, School of Science, Westlake University, Hangzhou, China

5 Institute of Natural Sciences, Westlake Institute for Advanced Study, Hangzhou, China

6 These authors contributed equally to this work

*E-mail: wangjianhui@westlake.edu.cn, liushi@westlake.edu.cn

Contents

1. Experimental details	1
1.1 Electrolyte preparations	1
1.2 Raman characterizations	2
1.3 Nuclear Magnetic Resonance (NMR) measurements	2
1.4 Compatibility tests between the electrolytes with the anode materials	3
2. Computational details	5
3. Supplementary Figures	6
4. Supplementary Tables	21
5. Supplementary References	26

1. Experimental details

1.1 Electrolyte preparations

Five lithium salts including lithium bis(fluorosulfonyl)imide (LiFSI, Chemspec, battery grade), lithium bis(trifluoromethanesulfonyl)imide (LiTFSI, DodoChem, battery grade), lithium trifluoromethanesulfonate (LiOTf, DodoChem, battery grade), lithium tetrafluoroborate (LiBF₄, DodoChem, battery grade) and lithium hexafluorophosphate (LiPF₆, DodoChem, battery grade) were used as solutes. Thirty-six organic reagents labelled in **1-36** (see Table S1 for product information) were used as primary solvents (termed as Solv.I) or secondary solvents (termed as Solv.II). These solvents were dried by 3 Å molecular sieves for two days. All these chemicals were stored and handled in an Ar-filled glove box with O₂ and H₂O contents lower than 1 ppm.

The electrolyte samples were prepared by mixing salt and solvent in each given molar ratio to form a transparent solution with the help of a mixer (Thinky, AR-100). Typically, the mixture of the salt and solvent was sealed in a 5 ml sample vial and subjected to a mixing in the mixer at 2000 rpm. The solubilities of LiFSI salt in the 36 solvents were firstly tested as listed in Table 1. For saturated solutions, the samples were kept still for 1~3 days before measurement to check if any solid precipitated at room temperature. For those solvents with a high solubility of LiFSI, three concentrations of LiFSI-x[Solvent] solutions (x = 2, 5, 10) were prepared to study the effect of salt concentration on the solution structure. Based on the results, nine solvents (MP, AN, DMC, EC, DME, THF, ET, nAA, and DMSO) were selected as the primary solvents (Solv.I) to form LiFSI-2[Solv.I] salt-concentrated electrolytes because of their high solubilities of the lithium salts and easy recognition of coordination states in Raman spectra. All the 36 solvents were used as the secondary solvent (Solv.II).

To determine the key parameter for screening the diluent for LHCEs, the salt-concentrated electrolytes of LiX-2[Solv.I] were diluted by eight equivalent secondary solvents (8[Solv.II]) to form 504 samples of LiX-2[Solv.I]-8[Solv.II] for structural characterizations, including 324

samples of LiFSI-2[Solv.I]-8[Solv.II] and 180 samples of LiX-2MP-8[Solv.II]. If the introduced Solv.II cannot fully dissolve into the concentrated electrolyte of LiX-2[Solv.I], leading to a solution stratification, the amount of Solv.II is reduced until a homogenous solution can be formed. The actual molar ratio values of Solv.II in the diluted sample of LiX-2[Solv.I]-8[Solv.II] are listed in the Fig. 3.

To quickly judge the soluble ability of a salt in a solvent, 180 samples of LiX-50[solvent] were prepared by introducing the five lithium salts in the 36 solvents with a salt-to-solvent molar ratio of 1 : 50. If all the lithium salt dissolves in the solvent to form a homogenous solution, this salt is regarded to be soluble in the solvent, otherwise it is regarded to be insoluble in the solvent.

1.2 Raman characterizations

Raman spectroscopy was measured by Cora-5700 Anton Paar with an exciting laser of 785 nm. The solution sample was sealed in a quartz cell to avoid any contamination from air. Raman spectra were recorded with 3 accumulated scans. Origin 2019b was applied to deconvolute the Raman peaks. The relative contents of coordinated and free-state species in the solution sample were quantitatively evaluated by comparing the total of corresponding deconvoluted Raman peak areas. For the electrolyte system of LiFSI-2MP-8[Solv.II], four states of MP molecules and FSI⁻ anions are recognized: “Free MP” at 850 cm⁻¹, “Coord. MP” at 870 cm⁻¹, “Free FSI⁻” at 730 cm⁻¹, and “Coord. FSI⁻” at 745 cm⁻¹. The contents of these four states are shown in Table S2.

1.3 Nuclear Magnetic Resonance (NMR) measurements

The two-dimensional Heteronuclear Overhauser effect spectroscopy (2D HOESY) allows to detect heteronuclear through-space NOE connectivities between nonbonded nuclei. ¹H-⁷Li HOESY experiments was recorded on a Bruker AVANCE NEO 500 MHz solution NMR

spectrometer equipped with a BBO Cryoprobe. The solution samples were used without adding any deuterium reagents to avoid any interference on the solution structure. All the NMR experiments were performed at 25 °C. A standard phase-sensitive pulse sequence (hoesyetgp.2) from the spectrometer library was used with a 2.5 s relaxation delay; four transients were collected with spectral widths of 8 ppm for ^1H and 5 ppm for ^7Li , and 128 data point in F1 and 2048 data points in F2. The 2D HOESY experiment was recorded with a mixing time of 500 ms.

Because the ratio of the HOE intensities of a pair of HOE signals is proportional to their ratio of internuclear distances¹, the internuclear distances (r_{target}) can be determined using a known reference distance (r_{ref}) and its HOE intensity (I_{ref}) according to Equation S1.

$$r_{target} = r_{ref} \sqrt[6]{\frac{I_{ref}}{I_{target}}} \quad \text{Equation S1}$$

Take LiFSI-2MP-8DCB as an example, five ^1H - ^7Li HOE cross peaks (marked as 1~5, see Fig. 1c) can be detected. The intensity of the strongest peak was set to 1.0000. And intensities of other peaks were analyzed using TopSpin version 3.6.2. Because the detected HOE signals were generated by the accumulated of multiple nuclei in corresponding group, the corrected HOE intensity of individual nucleus ($I_1\sim I_5$) can be then obtained by dividing its peak intensity with the atom number. The distances between Li^+ with H atoms of MP were labeled as r_1, r_2, r_3 corresponding to three different HOE peaks. Similarly, the distances of Li^+ with H atoms of DCB were labeled as r_4, r_5 . According to Equation S1, the ratio of above distances is $r_1:r_2:r_3:r_4:r_5 = \sqrt[6]{I_1^{-1}}:\sqrt[6]{I_2^{-1}}:\sqrt[6]{I_3^{-1}}:\sqrt[6]{I_4^{-1}}:\sqrt[6]{I_5^{-1}}$. Therein, r_2 was set as 1.00, then other relative distances can be calculated as listed in Table S3.

1.4 Compatibility tests between the electrolytes with the anode materials

The stability of lithium metal with the electrolytes was tested by soaking the polished lithium foils (5×5×1 mm) in the as-prepared electrolytes (5 mL) in a sealed sample vial. The changes

of the lithium foils and electrolytes were recorded with the time.

The compatibility of the graphite electrode with the electrolytes was tested in a graphite | Li half-cell using a galvanostatic charge/discharge operation. The graphite electrode was prepared following three steps: 1) mixing natural graphite (SEC Carbon Ltd.) and polyvinylidene difluoride (PVdF) in N-methylpyrrolidone (NMP) with a weight ratio of 90:10 (graphite : PVdF) to form a slurry, 2) casting the slurry onto the Cu current collector with a scraper, and 3) drying the graphite electrode at 120 °C under vacuum for 12 h. The obtained graphite electrode has a mass loading of active material of about 1.5 mg cm⁻². Graphite|Li half cells were assembled by the standard 2032-type coin cell hardware in an Ar-filled glove box. The volume of electrolyte in a coin cell was about 40 μL. The galvanostatic charge and discharge measurements were conducted by a battery test station (Neware, CT-4008) at 25 °C. All the cells were operated at a charge/discharge rate of 0.2C in a voltage range from 0.1 to 2.5 V. 1C-rate corresponds to 372 mA g⁻¹ on the weight basis of the graphite electrode.

2. Computational details

The atomistic solution structure of electrolyte was obtained from *ab initio* molecular dynamics (AIMD) simulations based on density functional theory as implemented in the Vienna ab initio Simulation Package (VASP)^{2,3}. The projector augmented wave (PAW)⁴ method was used to simulate the electron-ion interaction. And the exchange-correlation energy functional was treated within the generalized gradient approximation (GGA) using the Perdew-Burke-Ernzerhof (PBE) parametrization⁵ combined with D3 dispersion correction⁶. The cutoff energy and convergence criteria for electronic computation were set to 400 eV and 1×10^{-6} eV, respectively. Cubic simulation boxes were used for AIMD simulations of liquid electrolytes with various compositions, the parameters of which are listed in Table S4. The Nosé-Hoover thermostat^{7,8} was adopted to control the temperature of *NVE* ensemble and only the Gamma point was sampled in the Brillouin zone. To obtain unbiased homogenous solution structure with fully mixed ions and solvents, we firstly ran simulations at 498K. The high-temperature configuration was then equilibrated at room temperature (298K). After 5 ps' equilibration, radial distribution functions were computed from trajectories for at least 10 ps. The coordination energy ΔE shown in Fig. 4b was calculated by General Atomic and Molecular Electronic Structure System (GAMESS)⁹ using B3LYP functional^{10,11} and 6-31G* basis set.

3. Supplementary Figures

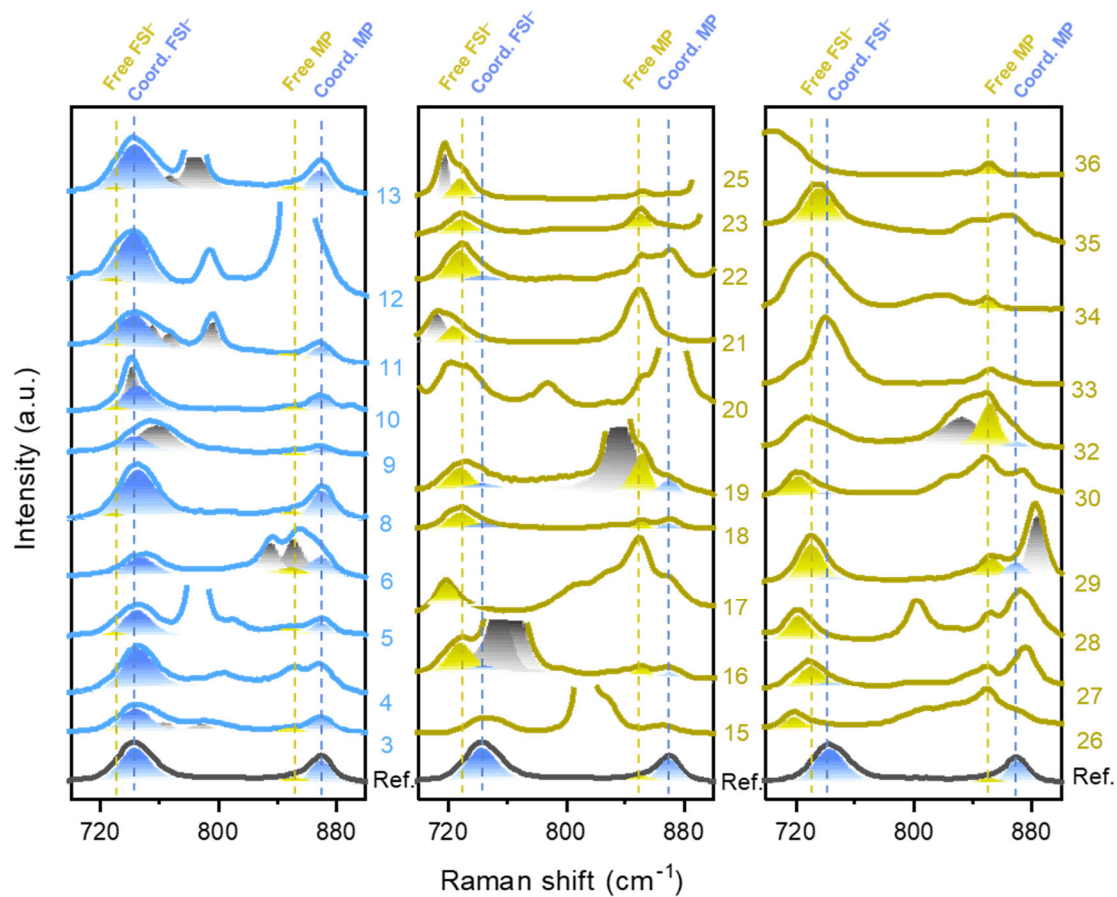


Fig. S1 | Raman spectra of LiFSI-2MP-8[Solv.II]. The label numbers of Solv.II for the electrolytes are shown on the Raman spectra; the numbers correspond to those listed in Table S1. Raman spectrum of the salt-concentrated electrolyte of LiFSI-2MP is used as the reference.

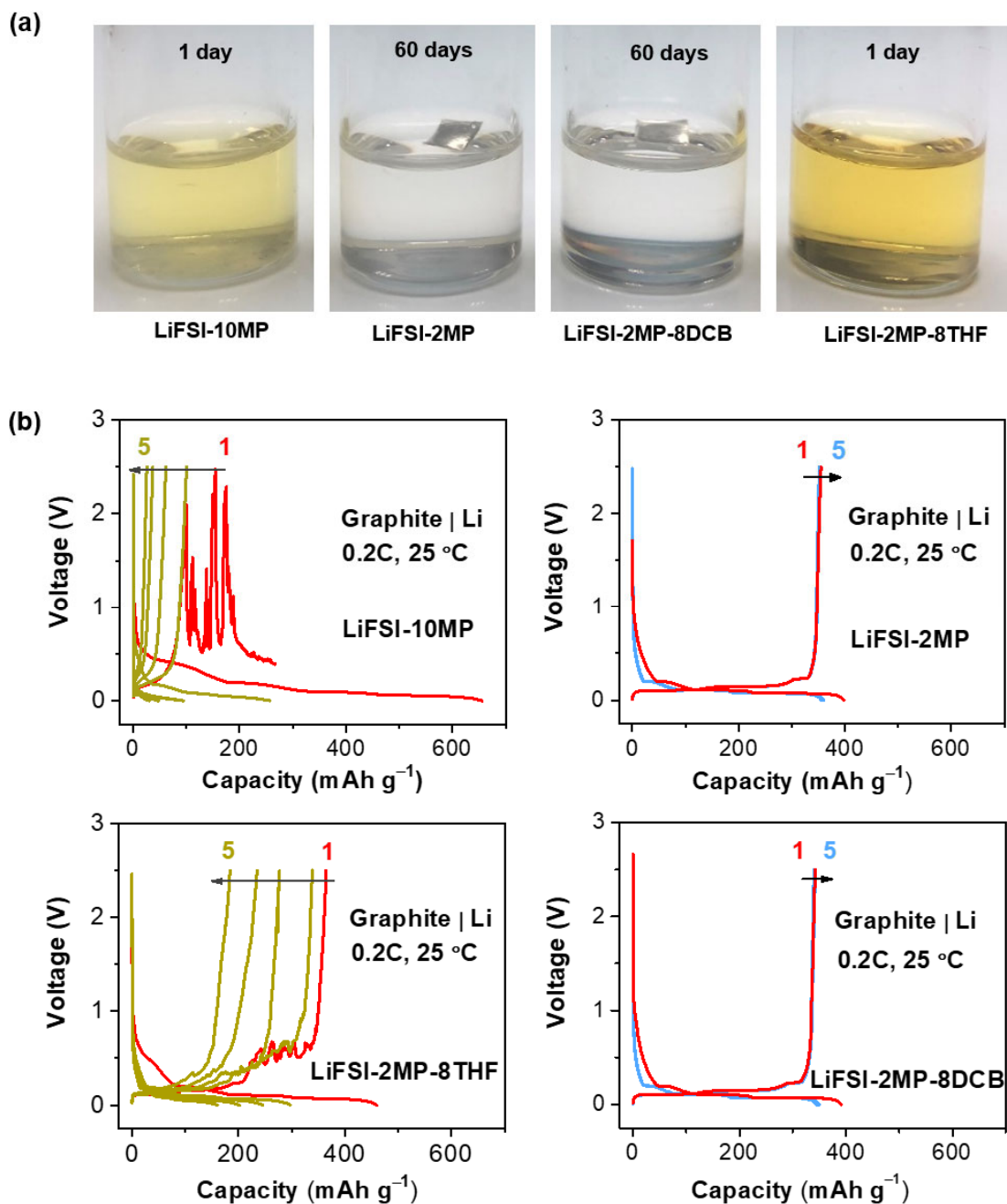


Fig. S2 | Compatibility tests of lithium metal and graphite electrodes in various electrolytes. (a) Lithium metal soaking in diluent (LiFSI-10MP), concentrated (LiFSI-2MP), and diluted concentrated (LiFSI-2MP-8THF and LiFSI-2MP-8DCB) electrolytes. (b) Initial five charge-discharge cycles of graphite | Li half-cells in these electrolytes. Obviously, the solutions of LiFSI-2MP and LiFSI-2MP-8DCB show quite stable with lithium metal and enable highly reversible lithium inter/de-intercalation reactions on the graphite electrode while the solutions of LiFSI-10MP and LiFSI-2MP-8THF cannot. These results confirm that the solution structure of the salt-concentrated electrolyte and its advanced properties could be reserved by introducing an appropriate diluent.

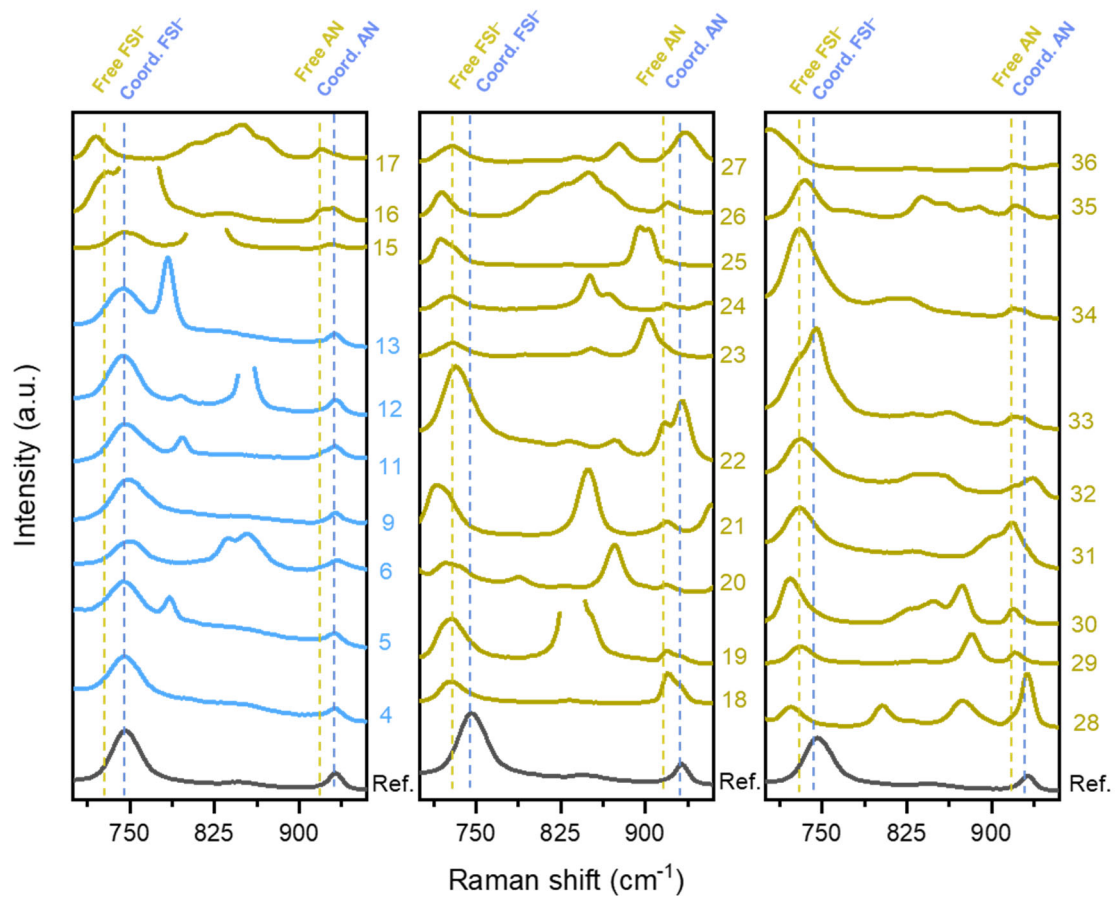


Fig. S3 | Raman spectra of LiFSI-2AN-8[Solv.II]. The label numbers of Solv.II for the electrolytes are shown on the Raman spectra; the numbers correspond to those listed in Table S1. Raman spectrum of the salt-concentrated electrolyte of LiFSI-2AN is used as the reference.

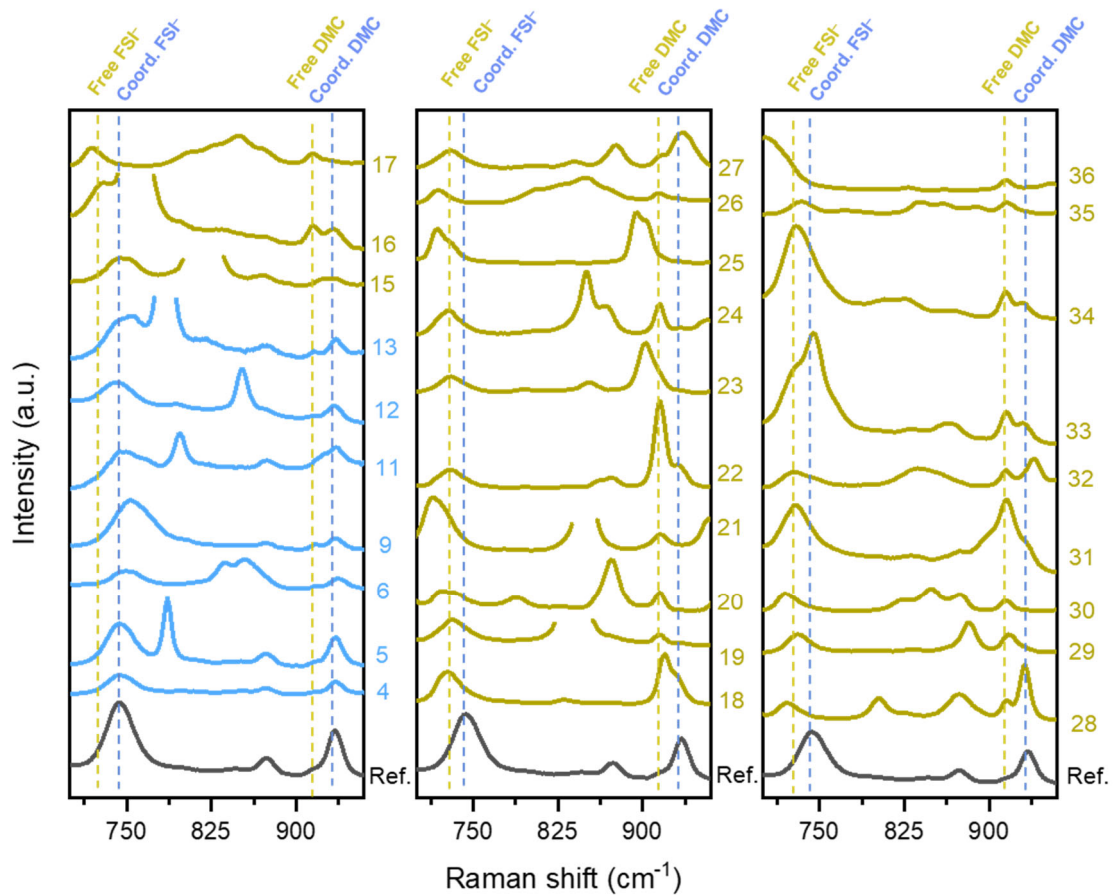


Fig. S4 | Raman spectra of LiFSI-2DMC-8[Solv.II]. The label numbers of Solv.II for the electrolytes are shown on the Raman spectra; the numbers correspond to those listed in Table S1. Raman spectrum of the salt-concentrated electrolyte of LiFSI-2DMC is used as the reference.

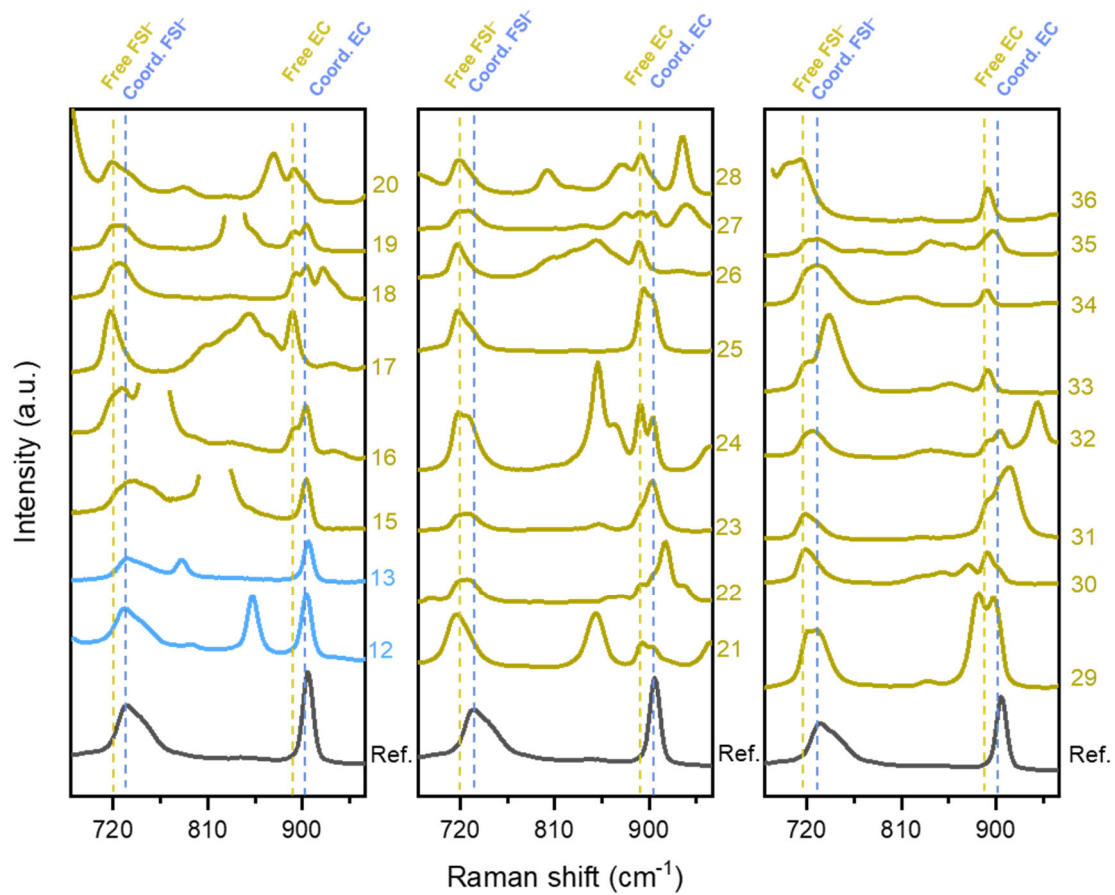


Fig. S5 | Raman spectra of LiFSI-2EC-8[Solv.II]. The label numbers of Solv.II for the electrolytes are shown on the Raman spectra; the numbers correspond to those listed in Table S1. Raman spectrum of the salt-concentrated electrolyte of LiFSI-2EC is used as the reference.

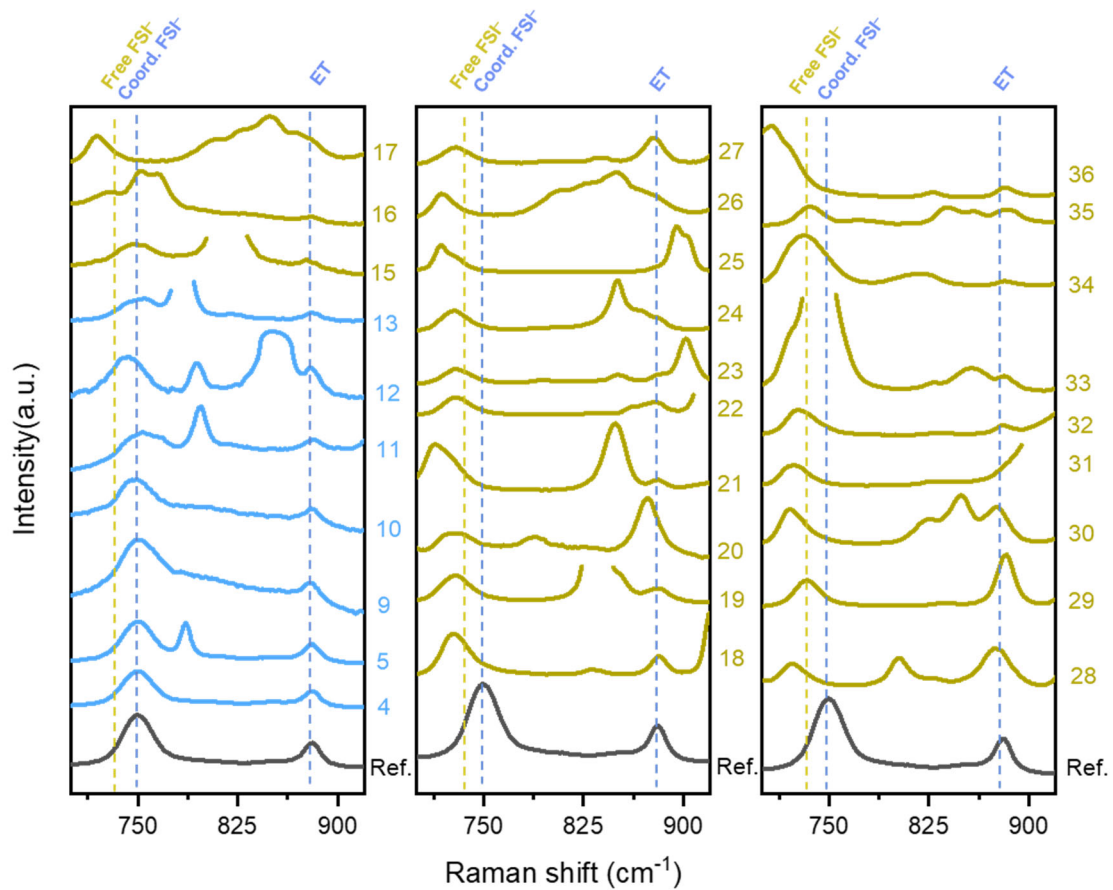


Fig. S6 | Raman spectra of LiFSI-2ET-8[Solv.II]. The label numbers of Solv.II for the electrolytes are shown on the Raman spectra; the numbers correspond to those listed in Table S1. Raman spectrum of the salt-concentrated electrolyte of LiFSI-2ET is used as the reference.

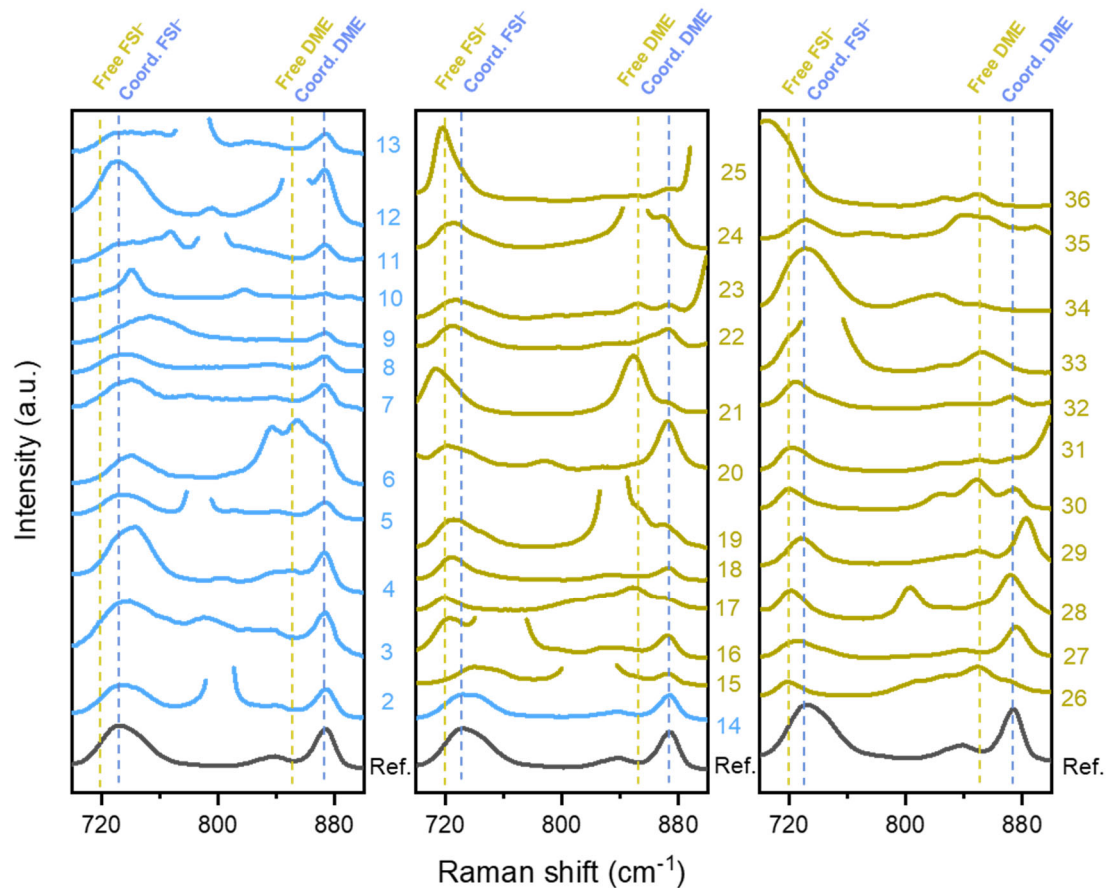


Fig. S7 | Raman spectra of LiFSI-2DME-8[Solv.II]. The label numbers of Solv.II for the electrolytes are shown on the Raman spectra; the numbers correspond to those listed in Table S1. Raman spectrum of the salt-concentrated electrolyte of LiFSI-2DME is used as the reference.

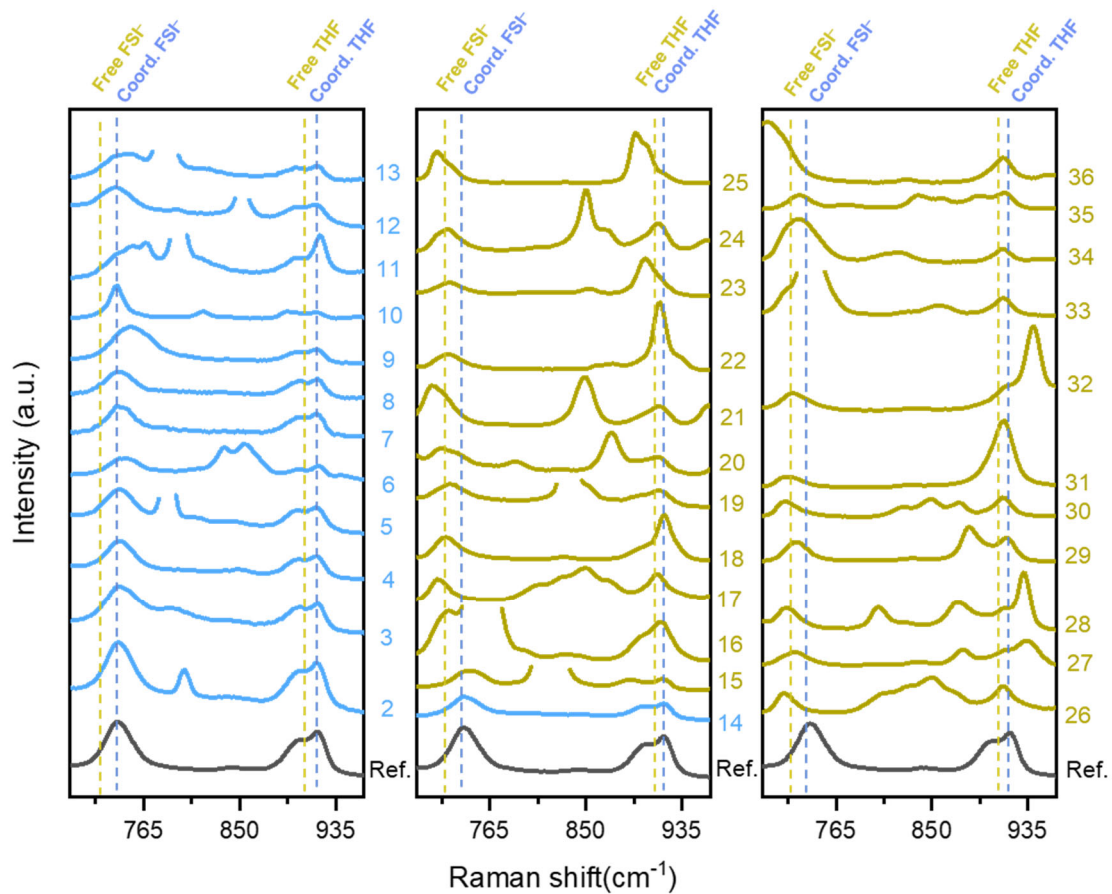


Fig. S8 | Raman spectra of LiFSI-2THF-8[Solv.II]. The label numbers of Solv.II for the electrolytes are shown on the Raman spectra; the numbers correspond to those listed in Table S1. Raman spectrum of the salt-concentrated electrolyte of LiFSI-2THF is used as the reference.

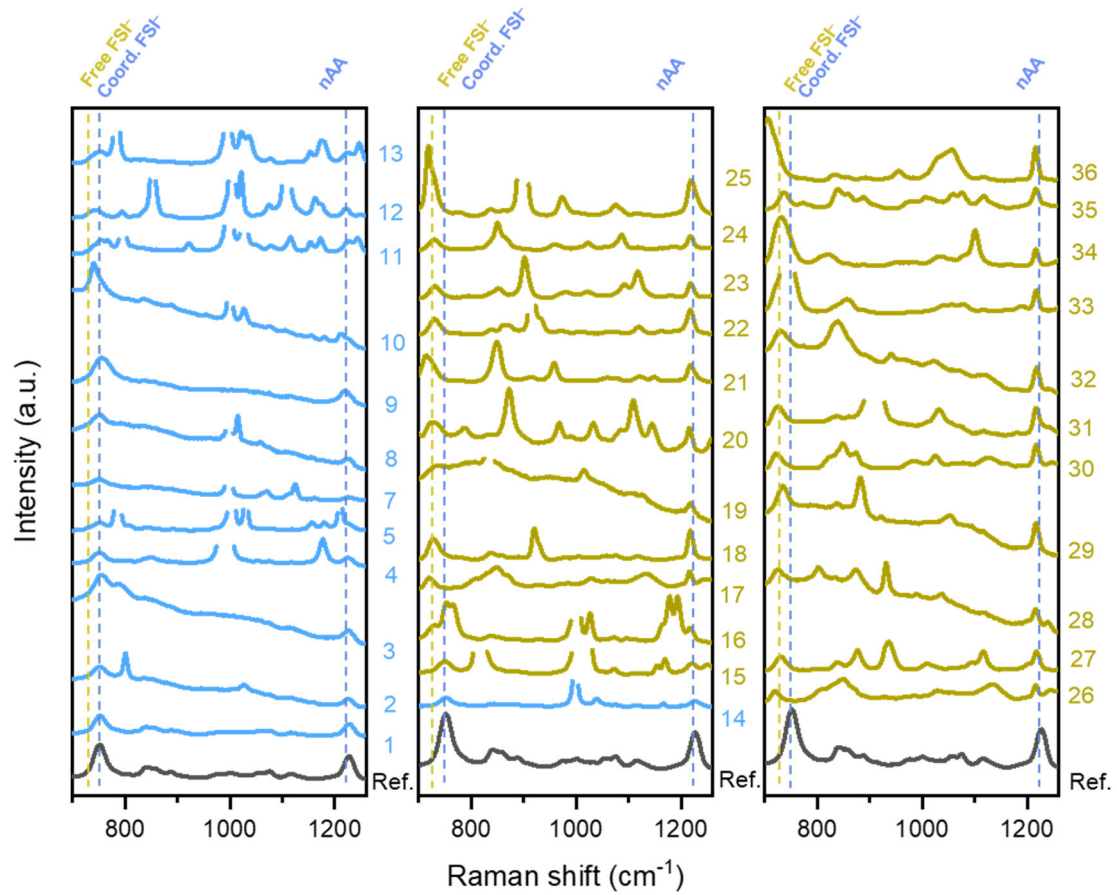


Fig. S9 | Raman spectra of LiFSI-2nAA-8[Solv.II]. The label numbers of Solv.II for the electrolytes are shown on the Raman spectra; the numbers correspond to those listed in Table S1. Raman spectrum of the salt-concentrated electrolyte of LiFSI-2nAA is used as the reference.

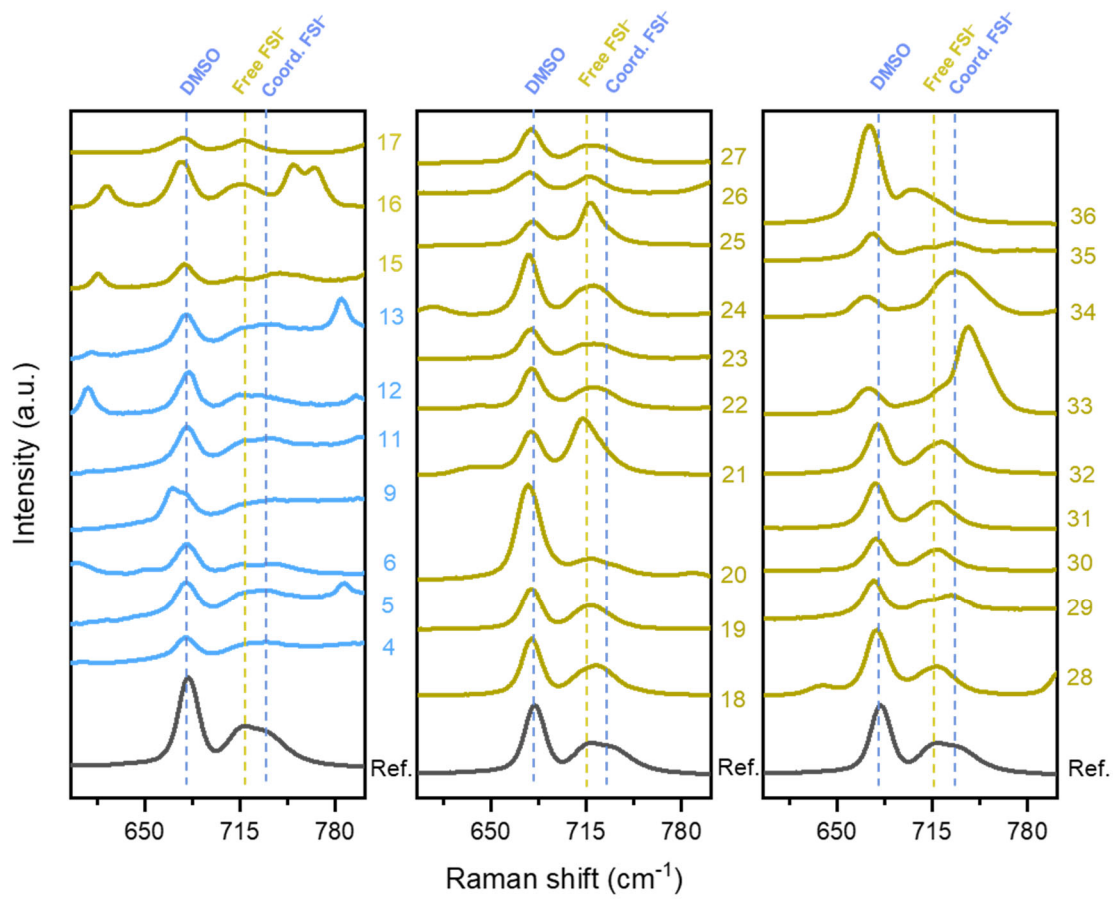


Fig. S10 | Raman spectra of LiFSI-2DMSO-8[Solv.II]. The label numbers of Solv.II for the electrolytes are shown on the Raman spectra; the numbers correspond to those listed in Table S1. Raman spectrum of the salt-concentrated electrolyte of LiFSI-2DMSO is used as the reference.

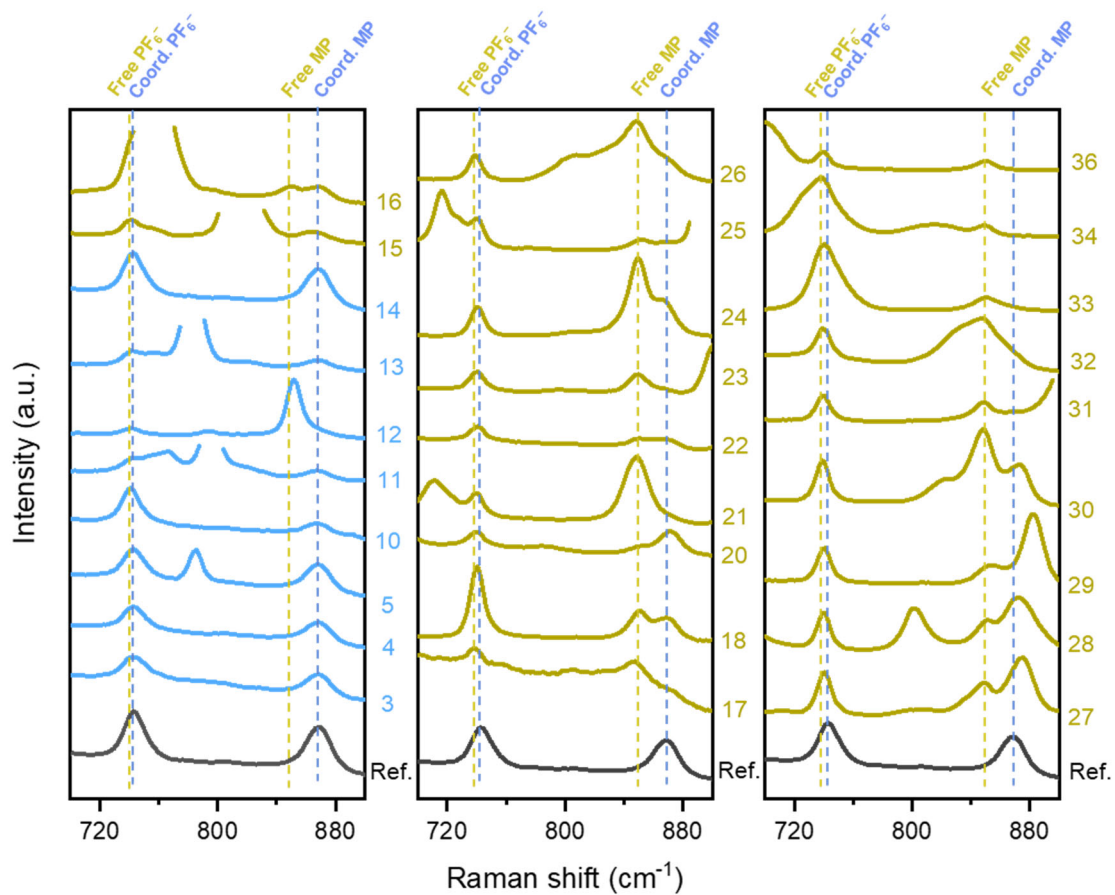


Fig. S11 | Raman spectra of LiPF₆-2MP-8[Solv.II]. The label numbers of Solv.II for the electrolytes are shown on the Raman spectra; the numbers correspond to those listed in Table S1. Raman spectrum of the salt-concentrated electrolyte of LiPF₆-2MP is used as the reference.

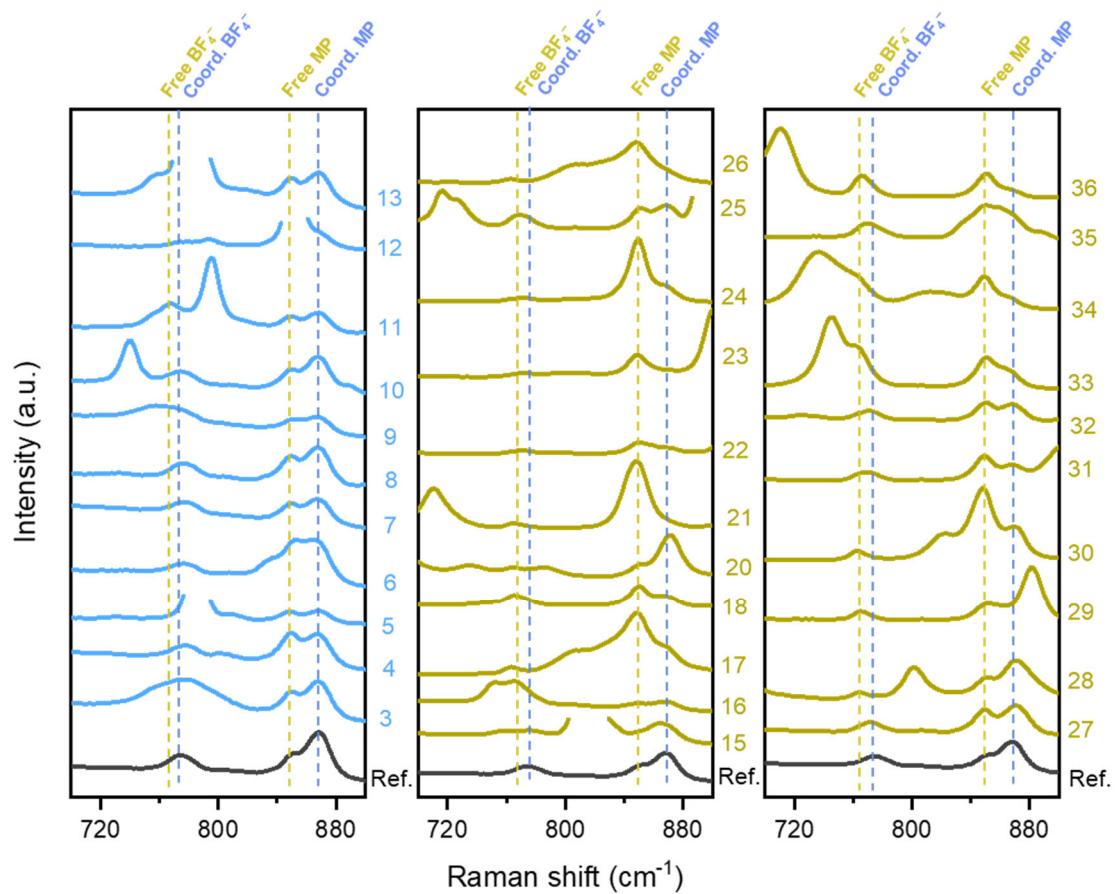


Fig. S12 | Raman spectra of LiBF₄-2MP-8[Solv.II]. The label numbers of Solv.II for the electrolytes are shown on the Raman spectra; the numbers correspond to those listed in Table S1. Raman spectrum of the salt-concentrated electrolyte of LiBF₄-2MP is used as the reference.

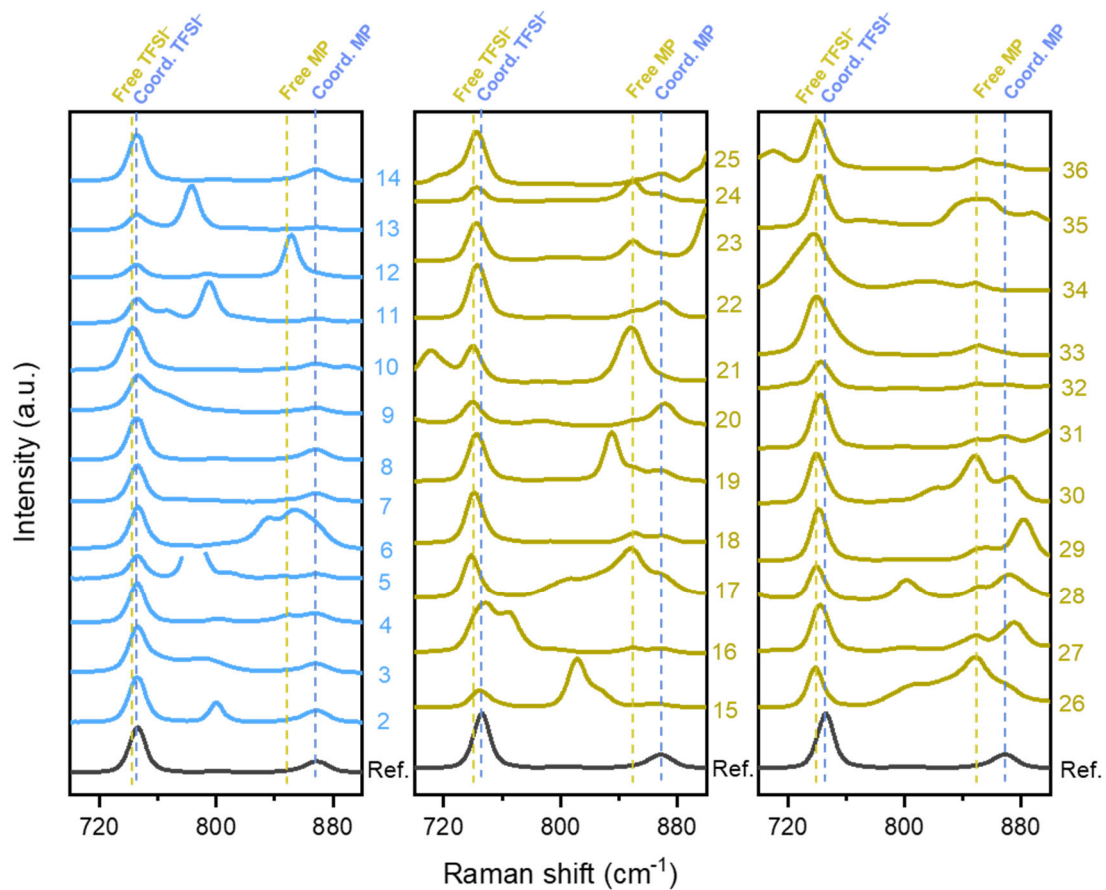


Fig. S13 | Raman spectra of LiTFSI-2MP-8[Solv.II]. The label numbers of Solv.II for the electrolytes are shown on the Raman spectra; the numbers correspond to those listed in Table S1. Raman spectrum of the salt-concentrated electrolyte of LiTFSI-2MP is used as the reference.

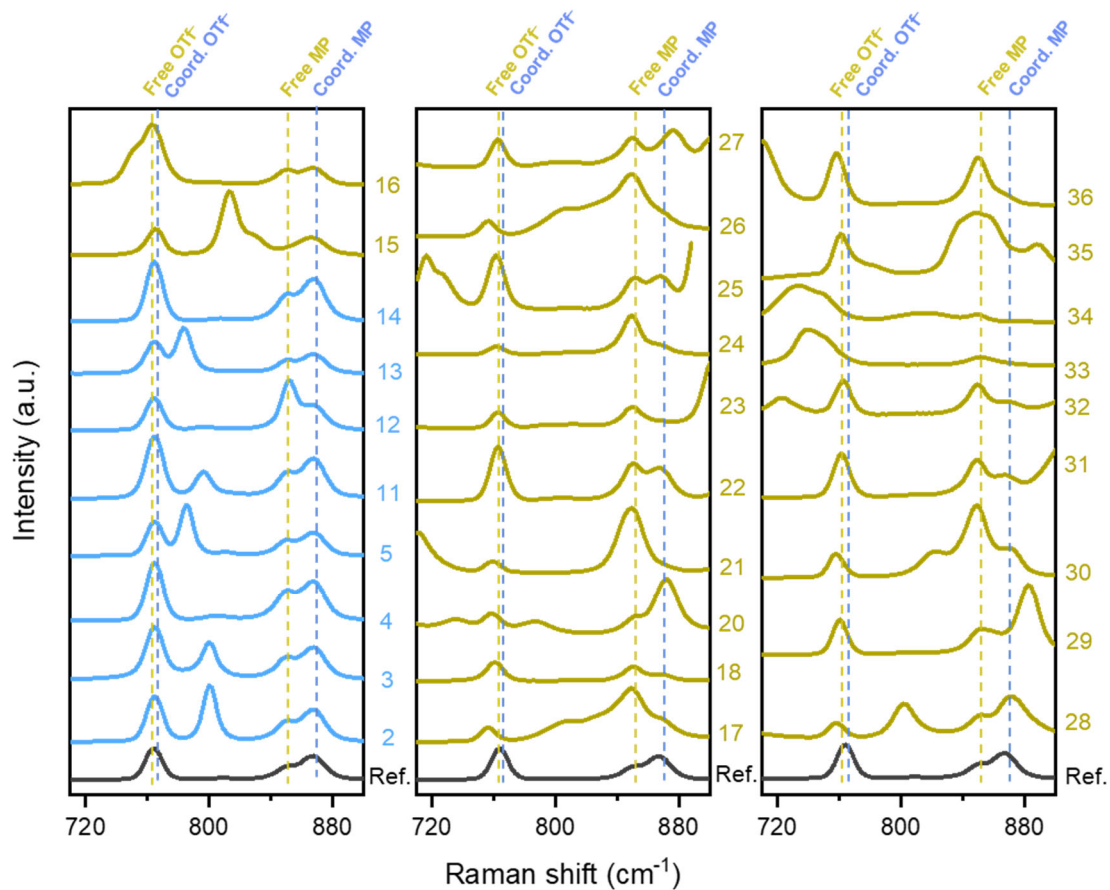


Fig. S14 | Raman spectra of LiOTf-2MP-8[Solv.II]. The label numbers of Solv.II for the electrolytes are shown on the Raman spectra; the numbers correspond to those listed in Table S1. Raman spectrum of the salt-concentrated electrolyte of LiOTf-2MP is used as the reference.

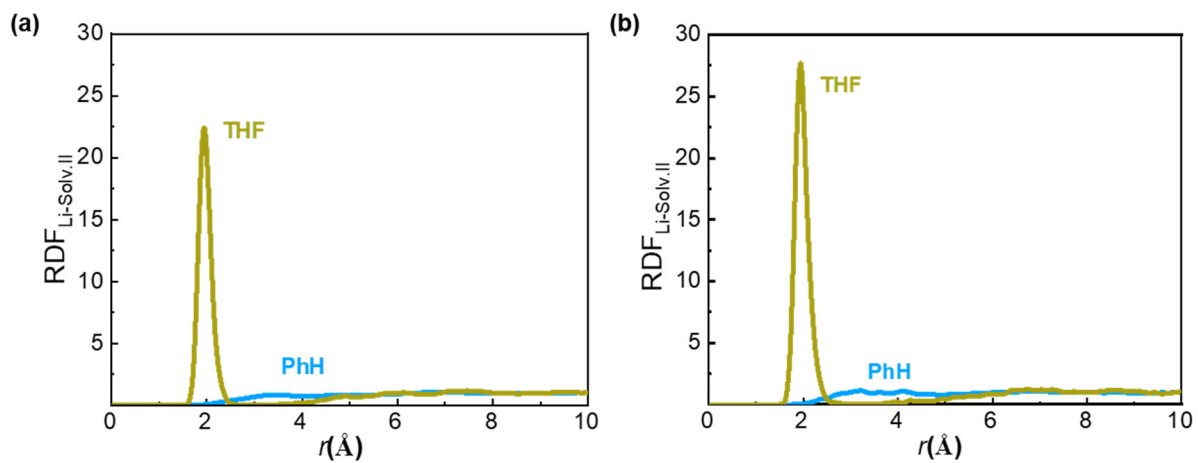
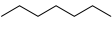
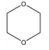
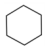
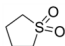
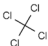
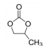

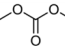
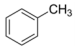
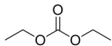
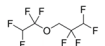
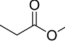
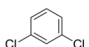
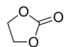
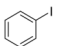
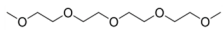
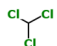
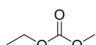


Fig. S15 | Comparisons of RDFs for Li-Solv. II pairs in LiX-2MP-2[Solv.II]. (a) $LiBF_4-2MP-2PhH$ and $LiBF_4-2MP-2THF$. **(b)** $LiOTf-2MP-2PhH$ and $LiOTf-2MP-2THF$. For these solutions with different anions, THF and PhH act as the co-solvent and diluent, respectively, consistent with the experimental results.

4. Supplementary Tables

Table S1 | Product information of the organic solvents involved in this work

Label	Solvents	CAS	Company	Purity/ grade	Label	Solvents	CAS	Company	Purity/ grade
1	 Heptane (HPT)	142-82-5	TCI	99.0%	19	 1,4-Dioxane (DOA)	123-91-1	TCI	99.0%
2	 Cyclohexane (CYH)	110-82-7	TCI	99.5%	20	 Tetramethylene sulfone (SL)	126-33-0	DodoChem	Battery grade
3	 Tetrachloromethane (CTC)	56-23-5	Adamas	99.5%	21	 Propylene carbonate (PC)	108-32-7	DodoChem	Battery grade
4	 Benzene (PhH)	71-43-2	TCI	99.5%	22	 Dimethyl carbonate (DMC)	616-38-6	DodoChem	Battery grade
5	 Toluene (TOL)	108-88-3	Adamas	99.8%	23	 Diethyl carbonate (DEC)	105-58-8	DodoChem	Battery grade
6	 1,1,2,2-Tetrafluoroethyl-2,2,3,3-Tetrafluoropropylether (TTE)	16627-68-2	DodoChem	Battery grade	24	 Methyl propanoate (MP)	554-12-1	Sigma-Aldrich	99.0%
7	 m-Dichlorobenzene (DCB)	541-73-1	Sigma-Aldrich	99.0%	25	 Ethylene carbonate (EC)	96-49-1	DodoChem	Battery grade
8	 Iodobenzene (IB)	591-50-4	TCI	99.0%	26	 Tetraethylene glycol dimethyl ether (G4)	143-24-8	DodoChem	Battery grade
9	 Chloroform (TCM)	67-66-3	Adamas	99.8%	27	 Ethyl Methyl Carbonate (EMC)	623-53-0	DodoChem	Battery grade

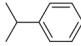
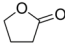
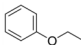
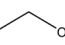
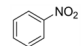
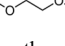
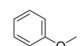
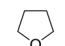
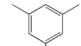
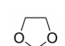
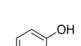
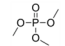
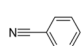
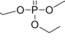
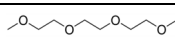
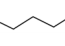
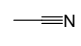
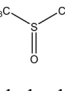
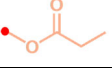
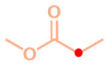
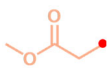
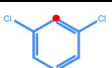
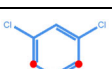
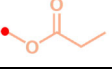
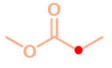
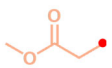


10	 Cumene (iPB)	98-82-8	TCI	99.0%	28	 γ -Butyrolactone (γ-BL)	96-48-0	Sigma-Aldrich	99.0%
11	 Phenetole (PhE)	103-73-1	Sigma-Aldrich	99%	29	 Ethanol (ET)	64-17-5	Adamas	99.9%
12	 Nitrobenzene (NB)	98-95-3	TCI	99.5%	30	 1,2-Dimethoxyethane (DME)	110-71-4	DodoChem	Battery grade
13	 Anisole (PhM)	100-66-3	TCI	99.0%	31	 Tetrahydrofuran (THF)	109-99-9	DodoChem	Battery grade
14	 Mesitylene (MES)	108-67-8	Adamas	99.0%	32	 1,3-dioxolane (DOL)	646-06-0	DodoChem	Battery grade
15	 Phenol (PhOH)	108-95-2	TCI	99.5%	33	 Trimethyl phosphate (TMP)	512-56-1	Sigma-Aldrich	99.0%
16	 Benzonitrile (BN)	100-47-0	TCI	99.0%	34	 Triethyl phosphate (TEP)	78-40-0	Sigma-Aldrich	99.8%
17	 Triethylene glycol monomethyl ether (G3)	112-49-2	DodoChem	Battery grade	35	 n-Amyl alcohol (nAA)	71-41-0	TCI	99.0%
18	 Acetonitrile (AN)	75-05-8	TCI	99.5%	36	 Dimethyl sulfoxide (DMSO)	67-68-5	DodoChem	Battery grade

Table S2 | Quantitative analysis results based on the deconvolution of Raman spectra of LiFSI-2MP-8[Solv.II]

Solv.II Label	Solv.II	FSI ⁻		MP	
		Free (%)	Coord. (%)	Free (%)	Coord. (%)
1	HPT	Immiscible	Immiscible	Immiscible	Immiscible
2	CYH	Immiscible	Immiscible	Immiscible	Immiscible
3	CTC	4.9	95.1	26.1	73.9
4	PhH	0.0	100.0	Overlapped	Overlapped
5	TOL	6.2	93.8	24.4	75.6
6	TTE	0.0	100.0	18.5	81.5
7	DCB	0.0	100.0	20.6	79.4
8	IB	2.4	97.6	17.3	82.7
9	TCM	0.0	100.0	23.6	76.4
10	iPB	6.4	93.6	26.7	73.3
11	PhE	7.4	92.6	14.1	85.9
12	NB	7.7	92.3	Overlapped	Overlapped
13	PhM	0.0	100.0	9.6	90.4
14	MES	Immiscible	Immiscible	Immiscible	Immiscible
15	PhOH	Overlapped	Overlapped	Overlapped	Overlapped
16	BN	88.9	11.1	68.0	32.0
17	G3	93.7	6.3	Overlapped	Overlapped
18	AN	71.8	28.2	62.4	37.6
19	DOA	84.6	15.4	69.0	31.0
20	SL	Overlapped	Overlapped	Overlapped	Overlapped
21	PC	96.2	3.8	Overlapped	Overlapped
22	DMC	85.3	14.7	Overlapped	Overlapped
23	DEC	88.2	11.8	95.1	4.9
24	MP	83.0	17.0	80.4	19.6
25	EC	93.5	6.5	72.9	27.1
26	G4	97.6	2.4	Overlapped	Overlapped
27	EMC	86.4	13.6	Overlapped	Overlapped
28	γ -BL	95.2	4.8	Overlapped	Overlapped
29	ET	85.3	17.4	58.6	41.4
30	DME	87.0	13.0	Overlapped	Overlapped
31	THF	84.7	15.3	87.8	12.2
32	DOL	Overlapped	Overlapped	93.9	6.1
33	TMP	Overlapped	Overlapped	Overlapped	Overlapped
34	TEP	Overlapped	Overlapped	100.0	0.0
35	nAA	100.0	0.0	Overlapped	Overlapped
36	DMSO	Overlapped	Overlapped	100.0	0.0

Table S3 | Calculation results of the relative distances between Li⁺ with Solv.I and with Solv.II in the electrolytes of LiFSI-2MP-8DCB and LiFSI-2MP-8THF according to the ¹H-⁷Li HOESY NMR spectra

Sample	Peak	Assignment (red tag)	<i>S</i>	<i>I</i>	<i>r</i>
LiFSI-2MP-8DCB	1		1.0000	<i>I</i> ₁ =0.3333	<i>r</i> ₁ =0.9(3)
	2		0.4422	<i>I</i> ₂ =0.2211	<i>r</i> ₂ =1.0(0)
	3		0.7078	<i>I</i> ₃ =0.2359	<i>r</i> ₃ =0.9(9)
	4		0.0215	<i>I</i> ₄ =0.0215	<i>r</i> ₄ =1.4(7)
	5		0.1533	<i>I</i> ₅ =0.0511	<i>r</i> ₅ =1.2(8)
LiFSI-2MP-8THF	1		0.4140	<i>I</i> ₁ =0.1380	<i>r</i> ₁ =1.0(1)
	2		0.2899	<i>I</i> ₂ =0.1450	<i>r</i> ₂ =1.0(0)
	3		0.4338	<i>I</i> ₃ =0.1446	<i>r</i> ₃ =1.0(0)
	4		1.0000	<i>I</i> ₄ =0.2500	<i>r</i> ₄ =0.9(1)
	5		0.5461	<i>I</i> ₅ =0.1365	<i>r</i> ₅ =1.0(1)

S: HOE intensity of corresponding ¹H-⁷Li cross peak, the intensity of the strongest peak was set to 1.0000.

I: corrected HOE intensity of individual nucleus, $I = S/\text{number of hydrogens in the corresponding functional group}$.

r: Relative distance of H-Li, $r \propto \sqrt[6]{I^{-1}}$, *r*₂ was set as 1.00.

Table S4 | The parameters of the electrolyte structures used in AIMD

	Experimental Density (g cm⁻³)	Length of cubic (Å)	Atomic number
8LiFSI-16MP-16PhH	1.15	18.21	496
8LiFSI-16MP-16THF	1.17	17.96	512
8LiBF₄-16MP-16PhH	1.04	17.66	464
8LiBF₄-16MP-16THF	1.06	17.34	480
8LiOTf-16MP-16PhH	1.08	18.20	488
8LiOTf-16MP-16THF	1.12	17.87	504

5. Supplementary References

- 1 Dewis, L., Crouch, R., Russell, D. & Butts, C. Improving the accuracy of H-1-F-19 internuclear distance measurement using 2D H-1-F-19 HOESY. *Magn. Reson. Chem.* **57**, 1143-1149 (2019).
- 2 Furthmüller, G. K. J. Efficiency of ab-initio total energy calculations for metals and semiconductors using a plane-wave basis set. *Comput. Mater. Sci.* **6**, 15-50 (1996).
- 3 Furthmüller, G. K. J. Efficient iterative schemes for ab initio total-energy calculations using a plane-wave basis set. *Phys. Rev. B* **54**, 11169-11186 (1996).
- 4 Blöchl, P. E. Projector augmented-wave method. *Phys. Rev. B* **50**, 17953-17979 (1994).
- 5 JP Perdew, K. B., M Ernzerhof. Generalized Gradient Approximation Made Simple. *Phys. Rev. Lett.* **77**, 3865-3868 (1996).
- 6 Grimme, S., Ehrlich, S. & Goerigk, L. Effect of the Damping Function in Dispersion Corrected Density Functional Theory. *J. Comput. Chem.* **32**, 1456-1465 (2011).
- 7 Nosé, S. A unified formulation of the constant temperature molecular dynamics methods. *J. Chem. Phys.* **81**, 511-519 (1984).
- 8 Hoover, W. G. Canonical dynamics: Equilibrium phase-space distributions. *Phys. Rev. A* **31**, 1695-1697 (1985).
- 9 Barca, G. M. J. et al. Recent developments in the general atomic and molecular electronic structure system. *J. Chem. Phys.* **152**, 154102 (2020).
- 10 Stephens, P. J. Chabalowski, C. F. Frisch, M. J. Ab Initio Calculation of Vibrational Absorption and Circular Dichroism Spectra Using Density Functional Force Fields. *J. Phys. Chem. C* **98**, 11623–11627 (1994).

11 Becke, A. D. Density-Functional Thermochemistry. III. The Role of Exact Exchange. *J. Chem. Phys.* **98**, 5648-5652 (1993).